A *Chlamydia* effector combining deubiquitination and acetylation activities induces Golgi fragmentation

Jonathan N. Pruneda[1], Robert J. Bastidas[2‡], Erithelgi Bertsoulaki[3‡], Kirby N. Swatek[1], Balaji Santhanam[4], Michael J. Clague[3], Raphael H. Valdivia[2], Sylvie Urbé[3], and David Komander[1*]

[1] Division of Protein and Nucleic Acid Chemistry, MRC Laboratory of Molecular Biology, Francis Crick Avenue, Cambridge CB2 0QH, UK.

[2] Department of Molecular Genetics and Microbiology, Duke University, Durham, NC 27710, USA

[3] Cellular and Molecular Physiology, Institute of Translational Medicine, University of Liverpool, Crown Street, Liverpool L69 3BX, UK.

[4] Division of Structural Studies, MRC Laboratory of Molecular Biology, Francis Crick Avenue, Cambridge CB2 0QH, UK.

‡ These authors contributed equally

* Correspondence to: David Komander, dk@mrc-lmb.cam.ac.uk

Pathogenic bacteria are armed with potent effector proteins that subvert host signaling processes during infection[1]. The activities of bacterial effectors and their associated roles within the host cell are often poorly understood, particularly for *Chlamydia trachomatis*[2], a WHO-designated neglected disease pathogen. We identify and explain remarkable dual Lys63-deubiquitinase (DUB) and Lys-acetyltransferase (AcT) activities in the *Chlamydia* effector ChlaDUB1. Crystal structures capturing intermediate stages of each reaction reveal how the same catalytic center of ChlaDUB1 can facilitate such distinct processes, and enable the generation of mutations that uncouple the two activities. Targeted *Chlamydia* mutant strains allow us to link the DUB activity of ChlaDUB1 and of the related, dedicated DUB ChlaDUB2 to fragmentation of the host Golgi apparatus, a key process in *Chlamydia* infection for which effectors have remained elusive. Our work illustrates the incredible versatility of bacterial effector proteins, and provides important insights toward understanding *Chlamydia* pathogenesis.

During infection, many Gram-negative pathogenic bacteria translocate effector proteins directly into host cells to modify signaling pathways important for invasion, survival, and replication. One particularly interesting family of effectors are those belonging to the CE clan of cysteine proteases. Members of this family were variously found to be proteases for ubiquitin-like (Ubl) modifiers, deubiquitinases (DUBs), or even Ser/Thr acetyltransferases (AcTs)[3,4,5,6,7,8,9,10,11], which is striking considering that they all share a structurally similar Cys protease fold. Physiologically, the activities are used against host inflammatory pathways. Deubiquitinases in particular are used by a wide range of pathogens to switch off

ubiquitin (Ub)-dependent inflammatory signaling processes[12], or interfere with microbe-directed autophagy (xenophagy) pathways. CE family DUBs such as *Legionella* SidE, *Salmonella* SseL, or *Chlamydia* ChlaDUB1 have been shown to mediate inhibition of autophagy, NF-κB signaling or cell death, during infection[10,13,14,15]. Similarly, the AcT activities of *Yersinia* YopJ and *Salmonella* AvrA modify phosphorylation sites, and directly block MAP kinase activation required for inflammatory signaling and innate immunity[7,8,9].

Recent phylogenetic analyses and crystal structures have started to explain the seemingly disconnected catalytic activities among CE family members, but the conundrum of the identical catalytic fold has remained intriguing. Indeed, a direct biochemical comparison of DUB and AcT activities in CE family proteins has not yet been performed. We used our panel of purified bacterial CE enzymes from a range of pathogens alongside their catalytically inactive variants (**Fig. 1a**) to test for DUB activity by monitoring cleavage of K63-linked diUb (**Fig. 1b**). In parallel, we tested for AcT activity by monitoring auto-acetylation via radioisotope incorporation following incubation with ^{14}C Acetyl-Coenzyme A (**Fig. 1c**). This analysis revealed *Salmonella* SseL, *Escherichia* ElaD, *Shigella* ShiCE, and *Rickettsia* RickCE to be dedicated DUBs, and identified *Legionella* LegCE, *Yersinia* YopJ, and *Salmonella* AvrA to be dedicated AcTs.

Remarkably, *Chlamydia* ChlaDUB1 could perform both DUB and AcT reactions, seemingly using the same catalytic Cys residue (compare **Fig. 1, b and c**). ChlaDUB1 is phylogenetically distinct from the YopJ-like family[11], but showed similar rates of auto-acetylation compared to YopJ and AvrA (although YopJ acetylation of

its substrate MEK2 (ref. [8]) is markedly faster, see **Supplementary Fig. 1a,b,c**). Importantly, ChlaDUB1 auto-acetylation occurs at Lys residues (**Supplementary Fig. 1d,e**) whereas YopJ-like family members predominantly target Ser/Thr residues[7,8,9]. Furthermore, ChlaDUB1 AcT activity is not regulated by phytic acid (inositol hexakisphosphate, IP6) (**Supplementary Fig. 1f,g**), in contrast to YopJ-like enzymes[16,17]. This identified ChlaDUB1 as a *bona-fide* Lys-AcT in addition to being a Lys63-specific DUB.

To explain how ChlaDUB1 could perform two seemingly disparate chemical reactions, namely deubiquitination – a hydrolysis reaction, and acetylation – a condensation reaction, we determined crystal structures of the enzyme bound to Ub, and bound to Coenzyme A (CoA) at 1.9 Å and 2.1 Å resolution, respectively (**Fig. 1d and Supplementary Table 1**). The structures showed hardly any conformational changes between each other, or in comparison to previous apo structures (pdb-id 5HAG[11], 5B5Q[15]) with overall RMSDs <1 Å (**Fig. 1e and Supplementary Fig. 2a**), but revealed distinct binding sites for Ub and CoA.

The ChlaDUB1~Ub structure (**Supplementary Fig. 2b**) was obtained using the Ub activity based probe Ub-propargylamide (UbPA), which covalently links one Ub molecule into the enzymatic S1 site (**Supplementary Fig. 3**). ChlaDUB1 forms similar interactions with Ub as compared to other CE proteases[10,11,18,19,20], involving both the Ile44 and Ile36 hydrophobic patches of Ub (**Supplementary Fig. 2c,d**).

The ChlaDUB1~CoA structure (**Supplementary Fig. 2e**) revealed a disulfide bridge between the cofactor's cysteamine and the catalytic Cys, and identified a charge-

complementary binding site for CoA near the active site (**Supplementary Fig. 2f**). The ChlaDUB1 CoA binding site is distinct from the CoA binding sites of the YopJ-like effector HopZ1a[16] and arylamine N-acetyltransferases (NATs)[21] (**Supplementary Fig. 2g,h**), and also removed from the Ub binding site (**Supplementary Fig. 3**).

Both structures together reveal the importance of an inserted helix that is unique to ChlaDUB1 and not present in other CE enzymes from bacteria, viruses, or eukaryotes; we had previously annotated this element as Variable Region 3 (VR-3)[11]. One face of this VR-3 helix contacts the adenosine and phosphate groups of the CoA molecule (**Fig. 2a,b**). Remarkably, the opposite face of the VR-3 helix binds the Ile36-patch of Ub (**Fig. 2a,b, Supplementary Fig. 2i**). This arrangement enables both DUB and AcT activities to utilize the same active site (**Fig. 1d and Supplementary Fig. 4a,b**), via spatially separated, independent binding sites for Ub and CoA. Consistently, Ub compromises AcT activity, but when the Ub C-terminus is missing, auto-acetylation is restored (**Supplementary Fig. 4c**). Separate binding sites for Ub and CoA further enabled us to uncouple DUB and AcT activity. ChlaDUB1 AcT activity was strongly diminished by mutation of K268E (VR-3), or G272E without affecting DUB activity. In contrast, DUB activity was abrogated by I267R (VR-3) or I225A mutation, yet these mutants did not affect auto-acetylation (**Fig. 2a,c, and Supplementary Fig. 5a**).

The VR-3 helix is central to dual activities in *C. trachomatis* (*C.t.*) ChlaDUB1 and present in all *Chlamydia* ChlaDUB homologues, such as ChlaDUB of *C. abortus* (*C.a.*), a cattle pathogen that is transmissible to humans. A 1.5 Å crystal structure of *C.a.* ChlaDUB confirmed the register of the predicted VR-3 helix as shown in the

sequence alignment (**Fig. 2d, Supplementary Fig. 5d,e, and Supplementary Table 1**). Importantly, the Ub- and CoA-coordinating residues within VR-3 are not jointly conserved (**Fig. 2d**), and we hypothesized that *C.t.* ChlaDUB2 should be a dedicated DUB, while *C.a.* ChlaDUB should be a dedicated AcT. Indeed, these predictions could be confirmed biochemically (**Fig. 2e**,**f and Supplementary Fig. 5b,c**). Together, our data strongly suggested that *Chlamydia* species evolved ChlaDUB effectors with dual activities and potentially multiple functions.

Functional characterization of *Chlamydia* effectors has remained challenging, mostly due to the rudimentary tools available for genetic manipulation of *Chlamydia*[22]. Nonetheless, we set out to uncover roles for the DUB/AcT ChlaDUB1 and the dedicated DUB ChlaDUB2 utilizing mutant strains harboring catalytically inactive ChlaDUB1 and ChlaDUB2 variants. One strain, containing a mutation leading to an amino acid substitution in the ChlaDUB2 catalytic His residue (H203Y) that inactivates the enzyme (**Supplementary Fig. 6a**), was identified from a collection of chemically mutagenized *C. trachomatis* strains[23]. This strain was back-crossed to wild-type *C. trachomatis* and a clean recombinant strain harboring only the ChlaDUB2 H203Y variant was isolated (Cdu2-H203Y) (**Fig. 3a, Supplementary Table 2, 3**). For ChlaDUB1, we obtained a recently characterized ChlaDUB1 mutant strain[15] generated by transposon mutagenesis that introduced an early stop codon before the catalytic Cys residue (*cdu1*-Tn) (**Fig. 3a, Supplementary Table 2**).

The ChlaDUB1 and ChlaDUB2 loss of function strains left us in the privileged position to assess the effects of either enzyme on host biology, and on contributions to *Chlamydia* infection. The *cdu1*-Tn mutant strain did not significantly reduce the

number of infectious progeny in HeLa cells as compared to a wild-type strain. This was markedly different in A549 cells, a human adenocarcinomic lung epithelial cell line, in which infection with the *cdu1*-Tn mutant strain reduced progeny by 90% (**Fig. 3b**). The latter was comparable to the effect of this strain *in vivo* using a transcervical mouse model of infection, whereas primary human fimbriae cells showed a bacterial growth defect only after prior stimulation with interferon-γ[15]. Surprisingly, the Cdu2-H203Y strain showed little to no growth defect in either HeLa or A549 cell lines compared to its two parental strains (see Methods) (**Fig. 3b**), suggesting that ChlaDUB1, with its additional AcT activity, may play a unique role in *Chlamydia* infection.

Next, we inspected infected cells by confocal microscopy. A prominent feature of *Chlamydia*-infected cells is the fragmentation and subsequent redistribution of the Golgi apparatus into ministacks that surround the pathogen-containing vacuole (termed the inclusion) at approximately 20 hours post infection[24,25]. Because ChlaDUB1 and ChlaDUB2 are actively expressed and secreted at this time post infection and have been shown to localize to the outside of the inclusion membrane where they could interact with neighboring organelles[15,28], we used our *cdu1*-Tn and Cdu2-H203Y mutant strains to test for a contribution to Golgi redistribution following infection. Remarkably, at 26-hours post infection, both the *cdu1*-Tn and Cdu2-H203Y mutant strains showed a dramatic impairment in redistribution of the Golgi apparatus (**Fig. 3c-f and Supplementary Fig. 6b-e**). Since both ChlaDUB1 and ChlaDUB2 mutant strains affected host Golgi redistribution, this strongly suggested that DUB activity is required in this process. Moreover, the comparable individual impact of each mutant strain on Golgi redistribution (**Fig. 3e,f**) indicates either non-redundant

roles for each DUB, or a strict dose dependency on DUB-activity introduced by *Chlamydia* to invoke the observed cell biological effect. Finally, a similar extent of Golgi redistribution was seen in A549 but also HeLa cells, contrasting the different impact of ChlaDUB mutant strains on bacterial growth rates (compare **Fig. 3c-f** with **3b**). This lack of correlation had been observed previously in HeLa cells, e.g. with InaC that regulates Golgi redistribution without impacting generation of bacterial progeny[23].

Our data suggested that ChlaDUB1 and ChlaDUB2 may have unrecognized roles in manipulating Golgi morphology and dynamics, which was corroborated in a simplified system (**Fig. 4a**). Strikingly, we found that Golgi fragmentation was readily induced by sole expression of either ChlaDUB1 or ChlaDUB2 in HeLa cells (**Fig. 4b, Supplementary Fig. 7a,b, and Supplementary Fig. 8a,b**). Expression of wild-type ChlaDUB1 and (to a lesser extent) ChlaDUB2 resulted in significant Golgi fragmentation as measured either by the number or the size of Golgi-stained puncta. Importantly, active site mutations eliminated this effect, which was again more pronounced for ChlaDUB1 (**Fig. 4c,d, Supplementary Fig. 7c,d, and Supplementary Fig. 8c,d**). All ChlaDUB1 constructs showed an enriched localization to the Golgi apparatus, indicating that the introduced mutations exclusively affect activity (**Fig 4b, Supplementary Fig. 7b**). ChlaDUB2 appeared to primarily localize to the endoplasmic reticulum (**Supplementary Fig. 8e**), which could explain its reduced ability to induce Golgi fragmentation as compared to ChlaDUB1. Using our structure-guided mutations that separate ChlaDUB1 DUB and AcT function (**Fig. 2g and 4a**), the Golgi fragmentation could be assigned as a DUB-dependent effect: A DUB-deficient I267R mutant was as defective in Golgi

fragmentation as a catalytically-inactive C345A construct, while an AcT-deficient ChlaDUB1 K268E mutant retained its Golgi fragmenting capabilities (**Fig. 4b-d and Supplementary Fig. 7a-d**).

Together, we here unveil a remarkable case of protein moonlighting[29], wherein a bacterial effector, *C. trachomatis* ChlaDUB1, performs two distinct enzymatic activities within its catalytic site, leading to separable cellular functions. Single amino acid substitutions can toggle between the activities, and this is used by closely related orthologues and paralogues in this enzyme family to modulate function (**Fig. 2g**). We further establish that the DUB activities present in ChlaDUB1 and also in the dedicated DUB paralogue ChlaDUB2, are necessary and sufficient for the fragmentation of the host Golgi apparatus, a prerequisite to Golgi redistribution around the *Chlamydia* inclusion. This adds ChlaDUB1 and ChlaDUB2 to the limited list of effectors and host factors implicated in this striking cell biological phenomenon[23-27] (see **Supplementary Fig. 9**). In overexpression studies, ChlaDUB1 has also been implicated with inhibition of NF-κB signaling[13] and cell death[15], and it is tempting to speculate that some of these effects are conferred by the AcT activity of ChlaDUB1. While this requires further study, the importance of ChlaDUB1 for *Chlamydia* infectivity[15] and its unique enzymatic nature make it an interesting candidate for future *Chlamydia*-targeted therapeutics.

Methods

Cloning and molecular biology. Generation of *Salmonella* Typhimurium SseL, *Chlamydia trachomatis* ChlaDUB1, *Escherichia coli* ElaD, *Shigella flexneri* ShiCE, *Rickettsia bellii* RickCE, *Legionella pneumophila* LegCE, *Yersinia pestis* YopJ, and *Salmonella* Typhimurium AvrA constructs was described previously[11]. Sequences for *Chlamydia trachomatis* ChlaDUB2 and *Chlamydia abortus* ChlaDUB were obtained via gene synthesis (Life Technologies). Following amplification with KOD polymerase (EMD Millipore), the genes were inserted into the pOPIN-B or pOPIN-GFP vector[30] with the In-Fusion cloning method (Takara Bio USA). All mutagenesis was performed using the Quikchange method (Agilent).

Protein expression and purification. Expression and purification of SseL (24-340), ElaD (2-407), ShiCE (2-405), RickCE (378-691), LegCE (141-360), YopJ (1-288), and AvrA (1-288) has been described previously[11]. *C.t.* ChlaDUB1 (130-401), *C.t.* ChlaDUB2 (80-339), and *C.a.* ChlaDUB were expressed in *E. coli* Rosetta2 pLacI cells (Novagen) at 18˚C for 20 h following induction with 0.2 mM IPTG an OD_{600} of 0.8-1.0. Cells were harvested in 25 mM Tris (pH 7.4), 200 mM NaCl, 2 mM ß-mercaptoethanol (Buffer A) and subjected to one freeze-thaw cycle. EDTA-free Complete protease inhibitor tablets (Roche), DNase, and Lysozyme were added prior to lysis by sonication. The resulting lysate was centrifuged at 35000 x g for 25 min, and applied to Talon resin (Takara Bio USA). The resin was washed with Buffer A thoroughly prior to elution with Buffer A containing 250 mM imidazole. During overnight dialysis back to Buffer A at 4˚C, the His-tag was cleaved with His-3C protease. Following a reverse affinity step over regenerated Talon resin, the resulting protein was then concentrated (10,000 MWCO, EMD Millipore) and applied to a gel

filtration column (Superdex75, GE Healthcare) equilibrated in 25 mM HEPES (pH 8.0), 150 mM NaCl, 5 mM DTT. Pure protein-containing fractions were concentrated, aliquoted, and flash-frozen for storage at -80˚C.

Deubiquitinase assays. All enzymes were diluted to a '2x' concentration in 25 mM Tris (pH 7.4), 150 mM NaCl, 10 mM DTT and allowed to fully reduce for 20 min at room temperature. 6 μM diUb stocks were prepared in 100 mM Tris (pH 7.4), 100 mM NaCl, 10 mM DTT and mixed 1:1 with 2x enzyme prior to incubation at 37˚C. Samples were quenched in reducing LDS sample buffer (ThermoFisher), resolved by SDS-PAGE, and visualized using silver stain (BioRad).
Ub/Ubl KG-TAMRA protease assays were performed as described previously[11].

Acetylation assays. All enzymes were diluted to 5 μM in 25 mM HEPES (pH 8.0), 50 mM NaCl, 0.5 mM DTT and incubated with 60 μM [1-^{14}C] Acetyl-CoA (60 mCi/mmol, PerkinElmer) at 37˚C for the indicated time. The panel shown in Figure 1 and all subsequent assays with YopJ or AvrA additionally included 200 nM inositol hexakisphosphate (IP6). Reactions were quenched with reducing LDS sample buffer (ThermoFisher) and resolved by SDS-PAGE prior to staining with Coomassie. Gels were then dried and exposed to a Phosphor screen for several days prior to imaging on a Typhoon scanner (GE Healthcare). ^{14}C autoradiography intensity was quantified using ImageJ[31] and normalized to the Coomassie stain signal.

Protein crystallization. The ChlaDUB1 (130-401)~Ub complex was purified by gel filtration following an overnight reaction at room temperature with 2-fold molar excess Ub-PA suicide probe[32]. Native ChlaDUB1~Ub crystals were obtained using protein

prepared in 25 mM Tris (pH 7.4), 125 mM NaCl, 4 mM DTT and crystallized at 10 mg/mL in 0.1 M MES (pH 6), 20% PEG 6000, with a 400 nL sitting drop at 1:1 protein:precipitant ratio. SeMet ChlaDUB1~Ub crystals were obtained using protein at 7 mg/mL in 0.1 M HEPES (pH 7.1), 18% PEG 8K, with a 200 nL sitting drop at 1:1 protein:precipitant ratio. The ChlaDUB1~CoA complex was crystallized by addition of 2 mM CoA to 12 mg/mL ChlaDUB1, and mixing with 0.1 M HEPES (pH 7.2), 20% PEG 8000 at a 1:1 protein:precipitant ratio in a 400 nL sitting drop. *C. a.* ChlaDUB (108-377) was prepared in 25 mM HEPES (pH 8.0), 150 mM NaCl, 5 mM DTT and crystallized in 0.1 M Tris (pH 7), 0.2 M calcium acetate, 20% PEG 3000 with a 400 nL sitting drop at 1:1 protein:precipitant ratio. All crystals were cryoprotected with mother liquor containing 25% glycerol. Cryoprotectant for ChlaDUB1~CoA crystals also contained 5 mM CoA.

Data collection, structure determination, and refinement. Data were collected at 100K at the Diamond Light Source (DLS) beam lines I02, I03, and I04 (see **Supplementary Table 1**). Data collections were performed at 0.9798, 0.9795, and 0.9794 Å wavelength for the ChlaDUB1~Ub, ChlaDUB1~CoA, and *C.a.* ChlaDUB structures, respectively. Integration and scaling were performed using XDS[33] and Aimless[34], respectively. The ChlaDUB1~Ub structure was solved experimentally using a SeMet SAD dataset with PHENIX AutoSol and AutoBuild[35,36,37]. ChlaDUB1~CoA and *C.a.* ChlaDUB structures were solved using molecular replacement in Phaser[38] using the apo ChlaDUB1 structure (pdb id 5HAG). Iterative rounds of model building and refinement were performed using COOT[39] and PHENIX[35], respectively. Ramachandran statistics (favored/allowed/outliers) for the ChlaDUB1~Ub, ChlaDUB1~CoA, and *C.a.* ChlaDUB structures were 97.2/2.8/0,

97.4/2.6/0, and 98.0/2.0/0, respectively. All figures were generated using PyMOL (www.pymol.org).

Cell lines. HeLa, A549, and Vero cell lines were obtained from ATCC, where they were authenticated by morphology, karyotyping, and STR analyses. Stocks were routinely tested and confirmed negative for mycoplasma contamination.

Chlamydia growth conditions and infections. HeLa, A549, and Vero cells were grown in high glucose DMEM supplemented with L-glutamine, sodium pyruvate (Gibco, Life Technologies) and 10% FBS (Mediatech, CellGro), at 37 ºC in a 5% CO2 humidified incubator. All cells infected with *Chlamydia* were centrifuged at 3,500 rpm for half an hour at 10°C immediately upon infection.

Chlamydia strains. All *Chlamydia* strains (**Supplementary Table 2**) were derived from *C. trachomatis* LGV biovar L2 434/Bu (wild-type). The *cdu1*-Tn strain was generously provided by Scott Hefty (The University of Kansas) and described previously[15]. The *cdu2-G607A* (Cdu2-H203Y) allele was identified in a collection of chemically mutagenized *C. trachomatis* L2 434/Bu strains by whole genome sequencing of a collection of pooled mutant strains[23]. Strain CTL2M467 was identified to harbor the *cdu2-G607A* single nucleotide variant (SNV) by Sanger sequencing of the *cdu2* (CTL0246) locus. Vero cells seeded in a 6 well plate were infected with CTL2M467. At 48 hours post infection (hpi), cell monolayers were lysed by hypotonic lysis, lysates sonicated, and bacterial cells collected by centrifugation at 14,000 rpm for 15 minutes at 4 °C. Bacterial cell pellets were resuspended in 1X DNAse I buffer (New England Biolabs) and treated with 4 Units of DNAse 1 (New

England Biolabs) for 1 hour at 37 °C to deplete co-purifying Vero DNA. Following a wash with PBS buffer, total DNA was isolated with a DNA isolation kit (DNeasy tissue and blood kit, Qiagen, Valencia, CA) following the manufacturer's instructions. One μg of CTL2M467 enriched DNA was fragmented with NEBNext dsDNA Fragmentase (New England Biolabs) and DNA sequencing libraries prepared with a NEBnext DNA Library Prep Kit for Illumina according to manufacturer's instructions. Libraries were sequenced with the MiSeq DNA Sequencing Platform (Illumina, Inc. San Diego, CA) at the Duke University IGSP sequencing facility. Genome assembly and single nucleotide variant (SNV) identification was performed with Geneious version 6 (Biomatters, http://www.geneious.com/). The *C. trachomatis* L2 434/Bu genome (GenBank no. NC_010287) was used as reference sequence. All SNV's identified (**Supplementary Table 3**) were independently verified by Sanger sequencing. M467 rs22 was isolated from a backcross of parental strain CTL2M467 (rifampin resistant-Rif^R) with a spectinomycin resistant L2 434/Bu strain ($Spec^R$) as described previously[40]. Vero cells were co-infected with strains CTL2M467 (Rif^R) and L2 434/Bu ($Spec^R$) at an MOI of 3 and a ratio of 1:1. At 48 hpi, crude cell lysates prepared in SPG buffer (0.25 M sucrose, 10 mM sodium phosphate, 5 nM glutamic acid) were used to infect Vero cells seeded in a 6 well plate. At 2 hpi, an agarose/DMEM overlay supplemented with rifampin (200 ng/mL) and spectinomycin (200 μg/mL) was added to infected cells as previously described[40] and cells incubated for 14 days. Recombinant strains were isolated from twenty-four individual plaques and expanded in Vero cells. All recombinant strains were genotyped by PCR for presence of CTL2M467 parental non-synonymous SNVs (**Supplementary Table 3**). Recombinant strain number 22 (M467 rs22) was found to harbor only the parental

346 *cdu2-G607A* mutation (Cdu2-H203Y). *Chlamydia* strains were maintained as frozen
347 stocks in SPG buffer.
348
349 ***Chlamydia growth assays.*** HeLa and A549 cells were seeded in wells of two 96
350 well plates (input and output plates). Cells were infected with *Chlamydia* strains at an
351 MOI of 0.6. At 24 hpi, infected cells in input plate were fixed with ice cold Methanol
352 and stored in PBS. At 48 hpi, crude lysates in SPG were prepared from infected cells
353 in output plates and a series of 1/10 dilutions were used to immediately infect
354 corresponding HeLa or A549 cells seeded in wells of a 96 well plate. At 24 hpi, cells
355 were fixed with ice cold Methanol. Fixed cells were stained with rabbit anti-Slc1[41] and
356 Hoechst. Images from stained cells were captured on an EVOS cell imaging system
357 (ThermoFisher scientific) with a 20X objective. Inclusion forming units (IFUs) were
358 quantified using Image J (NIH). Output IFU's from each *Chlamydia* inoculum was
359 normalized to their respective input IFU's. *Chlamydia* IFU production was measured
360 from 3 independent biological replicates.
361
362 ***Visual and quantitative analysis of Golgi redistribution around Chlamydia***
363 ***inclusions***
364 *Imaging.* HeLa and A549 cells grown on glass coverslips were infected with
365 *Chlamydia* strains at MOIs of 0.8. At 26 hpi, cells were fixed with pre-warmed (37°C)
366 3% formaldehyde in PBS for 20 minutes at room temperature. All washes and
367 antibody staining's were performed with pre-warmed (37°C) PBS and antibody
368 solutions respectively. Fixed cells were stained with rabbit anti-Slc1[41] and mouse
369 anti-GM130 antibodies (BD Biosciences), and Hoechst. Z-stacks of stained cells

were captured on a Zeiss 880 inverted fluorescence microscope with a 63X objective (Zeiss).

Golgi redistribution quantification. For each Z-stack, maximum intensity Z-projections were generated with Image J (NIH). The length of Golgi (defined by GM130 staining) distributed around *Chlamydia* inclusions and the length of each inclusion perimeter (defined by Slc1 staining) were measured using the line tool from Image J (NIH). The ratio of Golgi length to inclusion perimeter length was determined, and values are expressed as a percent. Three independent experiments were performed to assess Golgi distribution. Golgi distribution was assessed from 6 fields for a total of 90 cells per independent experiment.

High-resolution imaging. Standard deviation Z-projections of captured images (see above) were generated and images minimally processed with Image J (NIH).

ChlaDUB expression in mammalian cells

Imaging. HeLa cells grown on glass coverslips were transfected with 1 µg of plasmid using Genejuice (EMD Millipore). At 23-hours post-transfection, cells were fixed with 4% paraformaldehyde, immunostained for GM130 (BD Biosciences 610822). Nucleic acids were stained with DAPI. Images were collected on a Nikon Eclipse Ti microscope with a Super Plan Fluor ELWD 40XC objective or a 3i Marianas spinning disk inverted confocal microscope with a 63X oil objective and a CMOS camera (Hamatsu). The images were then processed using SlideBook software and Photoshop CS4 Version 11.0 (Adobe).

Quantification of Golgi fragmentation. Images were converted from 16-bit to 8-bit binary using Fiji. Following selection of the region of interest, the number and surface area of Golgi-stained particles were quantified using the Analyze Particles tool of Fiji. A minimum of three independent experiments were performed to assess Golgi fragmentation, each consisting of ~65 counted cells. Multinucleated cells, as well as cells that were cycling through mitosis, were excluded from the analysis.

Western blotting. HeLa cells were transfected with 1 µg of plasmid using Genejuice (EMD Millipore). At 23-hours post-transfection, cells were lysed in RIPA buffer and the protein amount was assessed using the Pierce BCA Protein Assay Kit (Thermo). 20 µg of lysates were resolved by SDS-PAGE and transferred onto nitrocellulose. Membranes were blocked in 5% milk/TBST for 1 h and probed for GFP (sheep, 1:1000, made in-house) and actin (rabbit, 1:10,000, Sigma A2266) for 1 h at room temperature. The IRDye 680LT Donkey anti-Rabbit IgG (LI-COR 926-68023) and IRDye 800CW Donkey anti-Goat IgG (cross-reacts with sheep IgG, LI-COR 926-32214) secondary antibodies were used at a concentration of 1:10,000 in 5% milk. Membranes were scanned using a LI-COR CLx Odyssey system and the Image Studio software, and minimally processed in Photoshop CS4 Version 11.0 (Adobe).

Statistics. All statistical analyses were performed using GraphPad Prism 7.0. *Chlamydia* growth assays were analyzed using a two-tailed Welch's t-test, all other analyses used a two-tailed Mann-Whitney test. All experiments contained three biological replicates. Data from these replicates is either combined or plotted separately, as described in the figure legends.

Data availability. The data that support the findings in this study are available from the corresponding author upon request. Coordinates and structure factors for the ChlaDUB1~Ub, ChlaDUB1~CoA, and *C.a.* ChlaDUB structures have been deposited with the protein data bank accession codes 6GZS, 6GZT, and 6GZU respectively.

References

1. Lin, Y. H. & Machner, M. P. Exploitation of the host cell ubiquitin machinery by microbial effector proteins. *J. Cell Sci*. **130,** 1985-1996 (2017).

2. Bastidas, R. J. & Valdivia, R. H. Emancipating Chlamydia: Advances in the genetic manipulation of a recalcitrant pathogen. *Microbiol. Mol. Biol. Rev*. **80,** 411-427 (2016).

3. Rytkönen, A. *et al*. SseL, a *Salmonella* deubiquitinase required for macrophage killing and virulence. *Proc. Natl. Acad. Sci. U.S.A.* **104,** 3502-3507 (2007).

4. Misaghi, S. *et al*. *Chlamydia trachomatis*-derived deubiquitinating enzymes in mammalian cells during infection. *Mol. Microbiol.* **61,** 142-150 (2006).

5. Catic, A., Misaghi, S., Korbel, G. A., & Ploegh, H. L. ElaD, a deubiquitinating protease expressed by *E. coli*. *PLoS One* **2,** e381 (2007).

6. Chosed, R. *et al*. Structural analysis of *Xanthomonas* XopD provides insights into substrate specificity of ubiquitin-like protein proteases. *J. Biol. Chem.* **282,** 6773-6782 (2007).

7. Mukherjee, S. *et al*. *Yersinia* YopJ acetylates and inhibits kinase activation by blocking phosphorylation. *Science* **312,** 1211-1214 (2006).

8. Mittal, R., Peak-Chew, S. Y., & McMahon, H. T. Acetylation of MEK2 and IκB kinase (IKK) activation loop residues by YopJ inhibits signaling. *Proc. Natl. Acad. Sci. U.S.A.* **103,** 18574-18579 (2006).

9. Jones, R. M. *et al*. *Salmonella* AvrA coordinates suppression of host immune and apoptotic defenses via JNK pathway blockade. *Cell Host Microbe* **3,** 233-244 (2008).

10. Sheedlo, M. J. *et al*. Structural basis of substrate recognition by a bacterial deubiquitinase important for dynamics of phagosome ubiquitination. *Proc. Natl. Acad. Sci. U.S.A.* **112,** 15090-15095 (2015).

11. Pruneda, J. N. *et al*. Molecular basis for ubiquitin and ubiquitin-like specificities in bacterial effector proteases. *Mol. Cell* ***63*****,** 261-276 (2016).

12. Corn, J. E. & Vucic, D. Ubiquitin in inflammation: the right linkage makes all the difference. *Nat. Struct. Mol. Biol.* **21,** 297-300 (2014).

13. Le Negrate, G. *et al*. ChlaDub1 of *Chlamydia trachomatis* suppresses NF-kappaB activation and inhibitis IkappaBalpha ubiquitination and degradation. *Cell Microbiol.* **10,** 1879-1892 (2008).

14. Mesquita, F. S. *et al*. The *Salmonella* deubiquitinase SseL inhibits selective autophagy of cytosolic aggregates. *PLoS Pathog.* **8,** e1002743 (2012).

15. Fischer, A. *et al*. *Chlamydia trachomatis*-containing vacuole serves as deubiquitination platform to stabilize Mcl-1 and to interfere with host defense. *eLife*. **6,** e21465 (2017).

16. Zhang, Z. M. *et al*. Structure of a pathogen effector reveals the enzymatic mechanism of a novel acetyltransferase family. *Nat. Struct. Mol. Biol.* **23,** 847-852 (2016).

17. Mittal, R., Peak-Chew, S. Y., Sade, R. S., Vallis, Y., & McMahon, H. T. The acetyltransferase activity of the bacterial toxin YopJ of *Yersinia* is activated by eukaryotic host cell inositol hexakisphosphate. *J. Biol. Chem.* **285,** 19927-19934 (2010).

18. Reverter, D. & Lima, C. D. A basis for SUMO protease specificity provided by analysis of human senp2 and a senp2-SUMO complex. *Structure* **12,** 1519-1531 (2004).

19. Reverter, D. *et al*. Structure of a complex between NEDD8 and the Ulp/Senp protease family member Den1. *J. Mol. Biol.* **345,** 141-151 (2005).

20. Shen, L. *et al*. Structural basis of NEDD8 ubiquitin discrimination by the deNEDDylating enzyme NEDP1. *EMBO J.* **24,** 1341-1351 (2005).

21. Fullam, E. *et al*. Divergence of cofactor recognition across evolution: coenzyme A binding in a prokaryotic arylamine N-acetyltransferase. *J. Mol. Biol.* **375,** 178-191 (2008).

22. Sixt, B. S. & Valdivia, R. H. Molecular genetic analysis of *Chlamydia* species. *Annu. Rev. Microbiol.* **70,** 179-198 (2016).

23. Kokes, M. *et al*. Integrating chemical mutagenesis and whole-genome sequencing as a platform for forward and reverse genetic analysis of *Chlamydia*. *Cell Host Microbe* **17,** 716-725 (2015).

24. Heuer, D. *et al*. *Chlamydia* causes fragmentation of the Golgi compartment to ensure reproduction. *Nature* **457,** 731-735 (2009).

25. Dumoux, M. & Hayward, R. D. Membrane contact sites between pathogen-containing compartments and host organelles. *Biochim. Biophys. Acta, Mol. Cell Biol. Lipids*. **1861,** 895-899 (2016).

26. Wesolowski, J. *et al. Chlamydia* hijacks ARF GTPases to coordinate microtubule posttranslational modifications and Golgi complex repositioning. *mBio*. **8,** e02280-16 (2017).

27. Rejman Lipinski, A. *et al*. Rab6 and Rab11 regulate *Chlamydia trachomatis* development and golgin-84-dependent Golgi fragmentation. *PLoS Pathog.* **5,** e1000615 (2009).

28. Wang, X., Hybiske, K., & Stephens, R. S. Direct visualization of the expression and localization of chlamydial effector proteins within infected host cells. *Pathog. Dis.* **76,** fty011 (2018).

29. Henderson, B. An overview of protein moonlighting in bacterial infection. *Biochem. Soc. Trans.* **42,** 1720-1727 (2014).

--

30. Berrow, N. S. *et al*. A versatile ligation-independent cloning method suitable for high-throughput expression screening applications. *Nucl. Acids Res.* **35,** e45 (2007).

31. Schneider, C. A., Rasband, W. S., & Eliceiri, K. W. NIH Image to ImageJ: 25 years of image analysis. *Nat. Methods* **9,** 671-675 (2012).

32. Ekkebus, R. *et al*. On terminal alkynes that can react with active-site cysteine nucleophiles in proteases. *J. Am. Chem. Soc.* **135,** 2867-2870 (2013).

33. Kabsch, W. XDS. *Acta Crytallogr. D Biol. Crystallogr.* **66,** 125-132 (2010).

34. Evans, P. R. & Murshudov, G. N. How good are my data and what is the resolution? *Acta Crytallogr. D Biol. Crystallogr.* **69,** 1204-1214 (2013).

35. Adams, P. D. *et al*. PHENIX: a comprehensive Python-based system for macromolecular structure solution. *Acta Crytallogr. D Biol. Crystallogr.* **66,** 213-221 (2010).

36. Terwilliger, T. C. *et al*. Decision-making in structure solution using Bayesian estimates of map quality: the PHENIX AutoSol wizard. *Acta Crytallogr. D Biol. Crystallogr.* **65,** 582-601 (2009).

37. Terwilliger, T. C. *et al*. Iterative model building, structure refinement and density modification with the PHENIX AutoBuild wizard. *Acta Crytallogr. D Biol. Crystallogr.* **64,** 61-69 (2008).

38. McCoy, A. J. *et al*. Phaser crystallographic software. *J. Appl. Cryst.* **40,** 658-674 (2007).

39. Emsley, P., Lohkamp, B., Scott, W. G., & Cowtan, K. Features and development of Coot. *Acta Crytallogr. D Biol. Crystallogr.* **66,** 486-501 (2010).

40. Nguyen, B. D. & Valdivia, R. H. Virulence determinants in the obligate intracellular pathogen *Chlamydia trachomatis* revealed by forward genetic approaches. *Proc. Natl. Acad. Sci. U.S.A.* **109,** 1263–1268 (2012).

41. Chen, Y. S. *et al*. The *Chlamydia trachomatis* type III secretion chaperone Slc1 engages multiple early effectors, including TepP, a tyrosinephosphorylated protein required for the recruitment of CrkI-II to

573 nascent inclusions and innate immune signaling. *PLoS Pathog.* **10,** e1003954
574 (2014).
575

Correspondence and requests for materials can be addressed to David Komander, dk@mrc-lmb.cam.ac.uk

Acknowledgements

We thank members of our laboratories for reagents and advice, particularly Dr. Lee Dolat (Duke University) for his contribution to some preliminary *Chlamydia* infection work. Access to DLS was supported in part by the EU FP7 infrastructure grant BIOSTRUCT-X (contract no. 283570). Work in the D.K. lab was funded by the Medical Research Council (U105192732), the European Research Council (724804), and the Lister Institute for Preventive Medicine. J.N.P. was supported on an EMBO Long-Term Fellowship. Work in the R.H.V. lab was funded by the National Institute of Health (R01AI100759 to R.H.V.) and the National Institute of Allergy and Infectious Diseases (STI CRC U19 AI084044 to R.J.B. and R.H.V.). E.B. was supported by North West Cancer Research.

Author Contributions

Conceptualization, J.N.P. and D.K.; Investigation, J.N.P., R.J.B., E.B., K.N.S., L.D. and B.S.; Methodology, R.J.B., R.H.V., M.J.C., and S.U.; Writing, J.N.P. and D.K.; Funding Acquisition, D.K., R.H.V., R.J.B., S.U., and M.J.C.

Competing Interests statement

The authors declare no competing interests.

Figure 1: Identification of specialized and dual-function CE-clan enzymes

a) Panel of purified bacterial CE-clan enzymes and their catalytically inactive Cys-to-Ala mutants. **b)** Deubiquitinase assay monitoring cleavage of K63-linked diUb following overnight incubation. **c)** Acetyltransferase assay monitoring ^{14}C incorporation following a 2 h incubation of each protein with ^{14}C-labeled Acetyl-CoA. Below, histogram representation of the WT/CA ^{14}C incorporation ratio following normalization of the ^{14}C autoradiography signal to the Coomassie stain. The average of three replicate experiments is plotted. A WT/CA ratio of one indicates no AcT activity, and is denoted by a red dashed line. Gels in **a, b,** and **c** are representative of triplicate experiments. All uncropped gels are shown in Supplementary Fig. 10. Asterisks indicate appreciable DUB (**b**) or AcT (**c**) activity. **d)** ChlaDUB1 complex crystal structures that capture intermediate stages of deubiquitinase (*top*) and acetyltransferase (*bottom*) activities. Inlay, a representative view of the ChlaDUB1 active site showing the Cys-His-Asp catalytic triad and the Gln oxyanion hole.

Figure 2: Molecular dissection of dual deubiquitinase/acetyltransferase activities

a) Close-up of the ChlaDUB1:CoA (brown:green) and ChlaDUB1:Ub (tan:red) interfaces with key interacting residues shown in ball-and-stick. Hydrogen bonds are shown as dashed lines. **b)** Helical wheel diagram illustrating the amphipathic nature of the ChlaDUB1 VR-3 helix, and its interactions with Ub or CoA (colored in red and green, respectively). **c)** Deubiquitinase (*top*) and acetyltransferase (*bottom*) assays illustrating that while both activities require the catalytic Cys residue, mutations in the Ub-binding and CoA-binding regions separate the two functions. A representative gel is shown of triplicate experiments. **d)** Sequence alignment of the VR-3 helix for orthologous *Chlamydia* ChlaDUB enzymes. The catalytic His, CoA-binding (green) and Ub-binding (red) residues are marked, and additional contacts are listed. **e)** ^{14}C acetylation assay with the ChlaDUB orthologues from *C. trachomatis* (*C.t.* ChlaDUB2) and *C. abortus* (*C.a.* ChlaDUB). **f)** Deubiquitinase assay monitoring K63-linked diUb cleavage by the *Chlamydia* ChlaDUB orthologues. Gels in **e** and **f** are representative of triplicate experiments. All uncropped gels are shown in Supplementary Fig. 10. **g)** Schematic depicting how deubiquitinase and acetyltransferase functions can be separated either by structure-guided mutation or evolution as represented by the ChlaDUB orthologues.

Figure 3: ChlaDUB function is required for *C. trachomatis* Golgi fragmentation

a) Topology diagram illustrating *C.t.* ChlaDUB1 and *C.t.* ChlaDUB2 domain architecture, with active site residues annotated within the catalytic domains. Changes present in the *cdu1*-Tn and Cdu2-H203Y defective strains are shown above. **b)** *C. trachomatis* growth assay measured as inclusion forming units (IFU) output per IFU input following a 48 h infection in either HeLa or A549 cells. Values were normalized to 100% for wild-type. Statistical significance compared to parental controls was measured using a two-tailed Welch's t-test. HeLa: Wild-type – *cdu1*-Tn, p=0.768; Rif^R – Cdu2-H203Y, p=0.0195; $Spec^R$ – Cdu2-H203Y, p=0.392. A549: Wild-type – *cdu1*-Tn, p=0.000173; Rif^R – Cdu2-H203Y, p=0.615; $Spec^R$ – Cdu2-H203Y, p=0.791. n=3. **c)** Representative confocal images showing Golgi fragmentation and redistribution around the *Chlamydia* inclusion following a 26 h infection of HeLa cells. Samples were immunostained with anti-GM130 (cis-Golgi, red) and anti-Slc1 (*Chlamydia*, green) antibodies, and Hoechst stained (DNA, blue). Isolated channels for the boxed region are shown below, and full versions are shown in Supplementary Fig. 6b. Scale bar corresponds to 10 μm. **d)** As in c) for A549 cells. Full versions are shown in Supplementary Fig. 6c. **e)** Quantification of c) following measurement of Golgi distribution around the circumference of the *Chlamydia* inclusion in 90 cells for each of three independent replicates. Mean values are shown as a red bar with individual data points overlaid. Statistical significance compared to parental was measured using a two-tailed Mann-Whitney test. Wild-type – *cdu1*-Tn, p<1E-15; Rif^R – Cdu2-H203Y, p<1E-15; $Spec^R$ – Cdu2-H203Y, p<1E-15. Separated plots for each replicate are shown in Supplementary Fig. 6d. **f)** As in e) for A549 cells. Wild-type – *cdu1*-Tn, p<1E-15; Rif^R – Cdu2-H203Y, p<1E-15; $Spec^R$ – Cdu2-H203Y, p<1E-15. Separated plots for each replicate are shown in Supplementary Fig. 6e.

Figure 4: ChlaDUB deubiquitinase activity is required for *C. trachomatis* Golgi fragmentation

a) Topology diagram illustrating the constructs used to characterize activity dependence of Golgi fragmentation following expression of ChlaDUB1 in mammalian cells. Separation-of-function mutations were selected from structural and biochemical work discussed in Fig. 2. **b)** Representative confocal images showing Golgi fragmentation in HeLa cells following expression of GFP-tagged ChlaDUB1. Samples were immunostained with anti-GM130 (cis-Golgi, red) and DAPI stained (DNA, blue). GFP fluorescence is shown in green. Isolated channels for the boxed region are shown below, and full versions are shown in Supplementary Fig. 7b. Scale bar corresponds to 10 μm. **c)** Quantification of cis-Golgi-stained puncta from b) for ~65 cells in each of three independent replicates (two remaining replicates are plotted in Supplementary Fig. 7c). Mean values are shown as red bars with individual data points overlaid. Statistical significance compared to GFP control was measured using a two-tailed Mann-Whitney test. GFP – WT, p=2.53E-8; GFP – C345A, p=0.386; GFP – I267R, p=0.0253; GFP – K268E, p=2E-15. **d)** Measurement of cis-Golgi-stained puncta size from b) for ~65 cells in each of three independent replicates (two remaining replicates are plotted in Supplementary Fig. 7d). Mean values are shown as red bars, median values are shown as black bars inside a quartile box plot, with individual data points overlaid. Statistical significance compared to GFP control was measured using a two-tailed Mann-Whitney test. GFP – WT, p=6.26E-12; GFP – C345A, p=0.0489; GFP – I267R, p=0.357; GFP – K268E, p=4.32E-10.

Figure 1: Identification of specialized and dual-function CE-clan enzymes

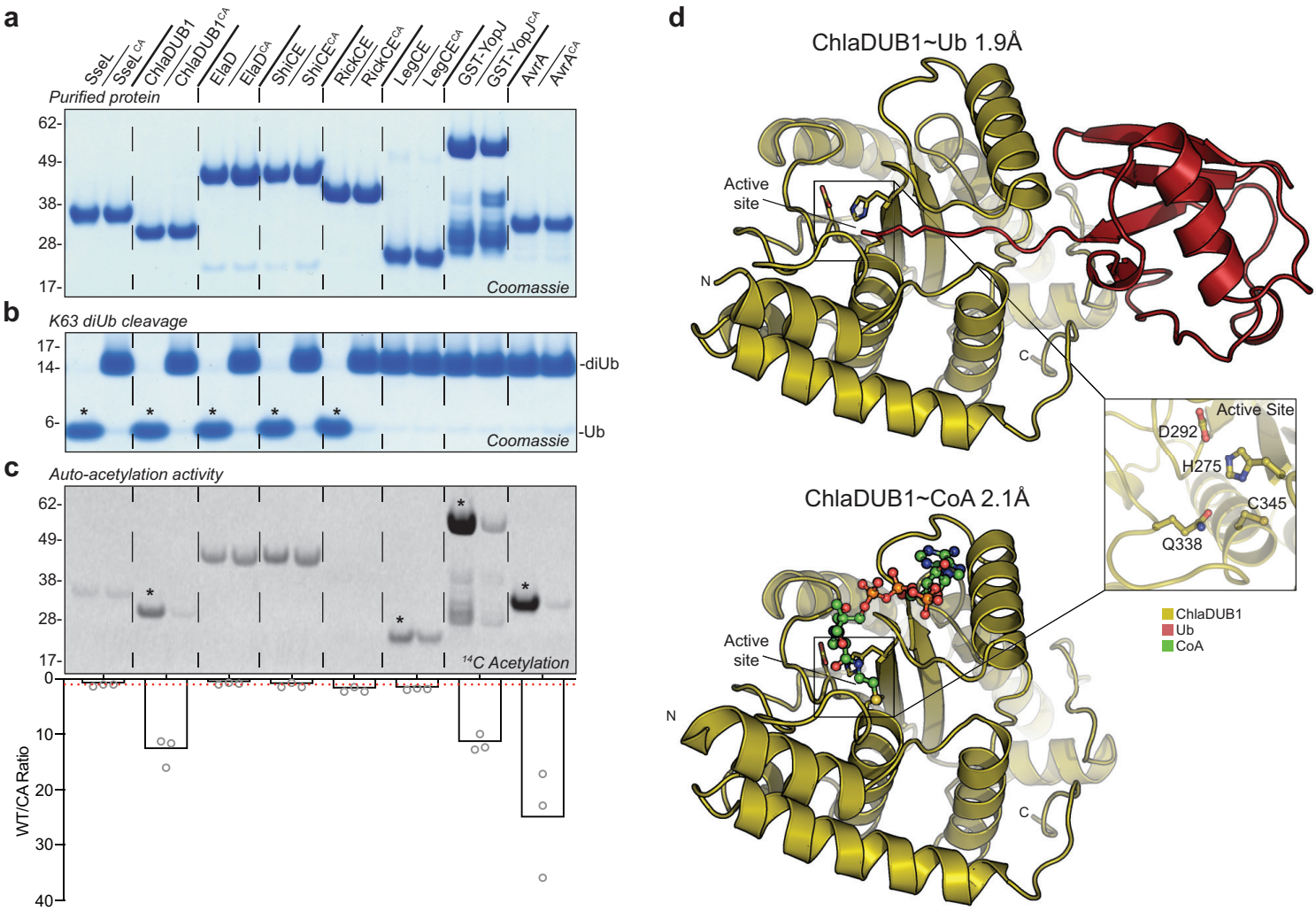

Figure 2: Molecular dissection of dual deubiquitinase/acetyltransferase activities

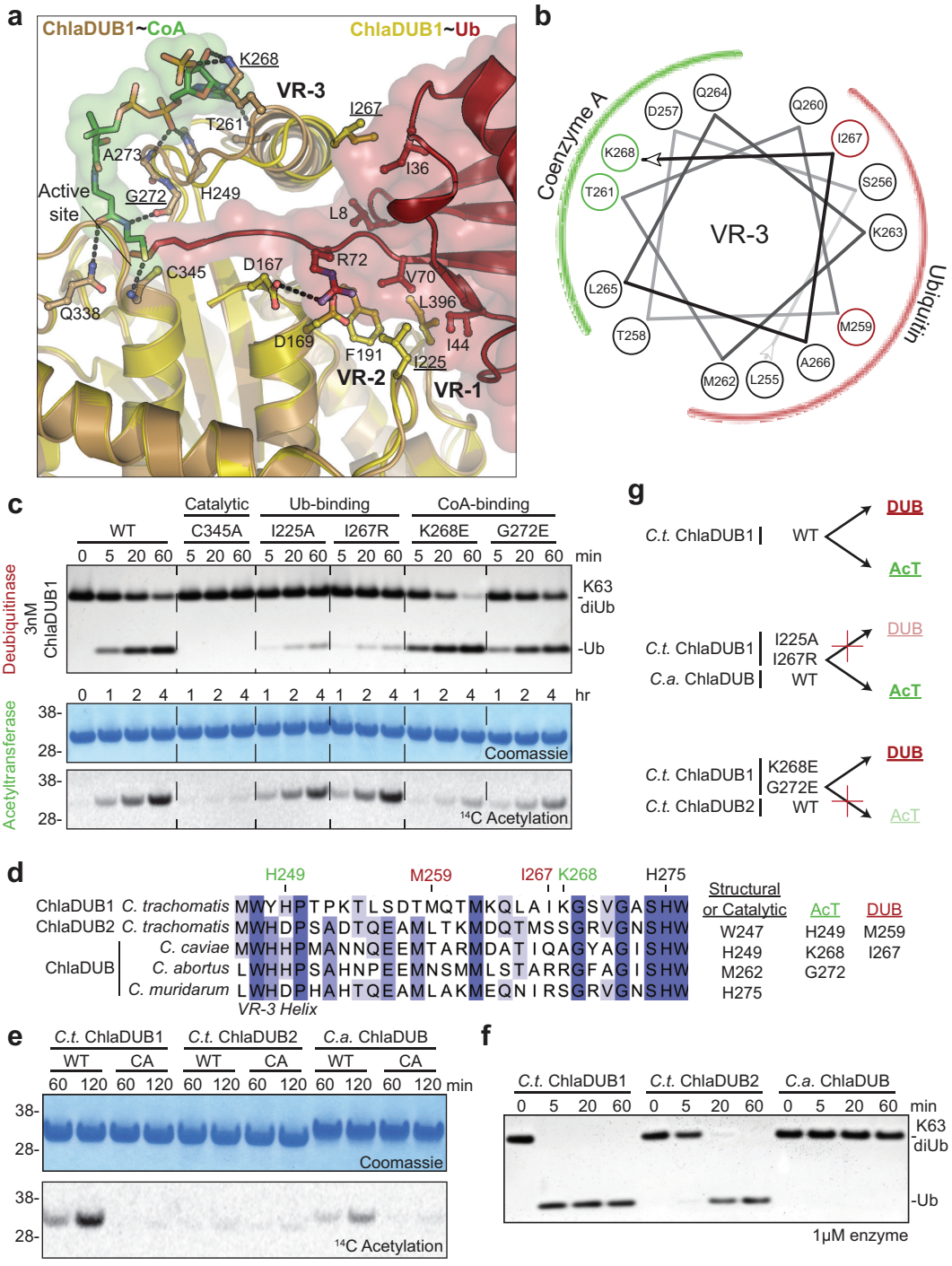

Figure 3: ChlaDUB function is required for *C. trachomatis* Golgi fragmentation

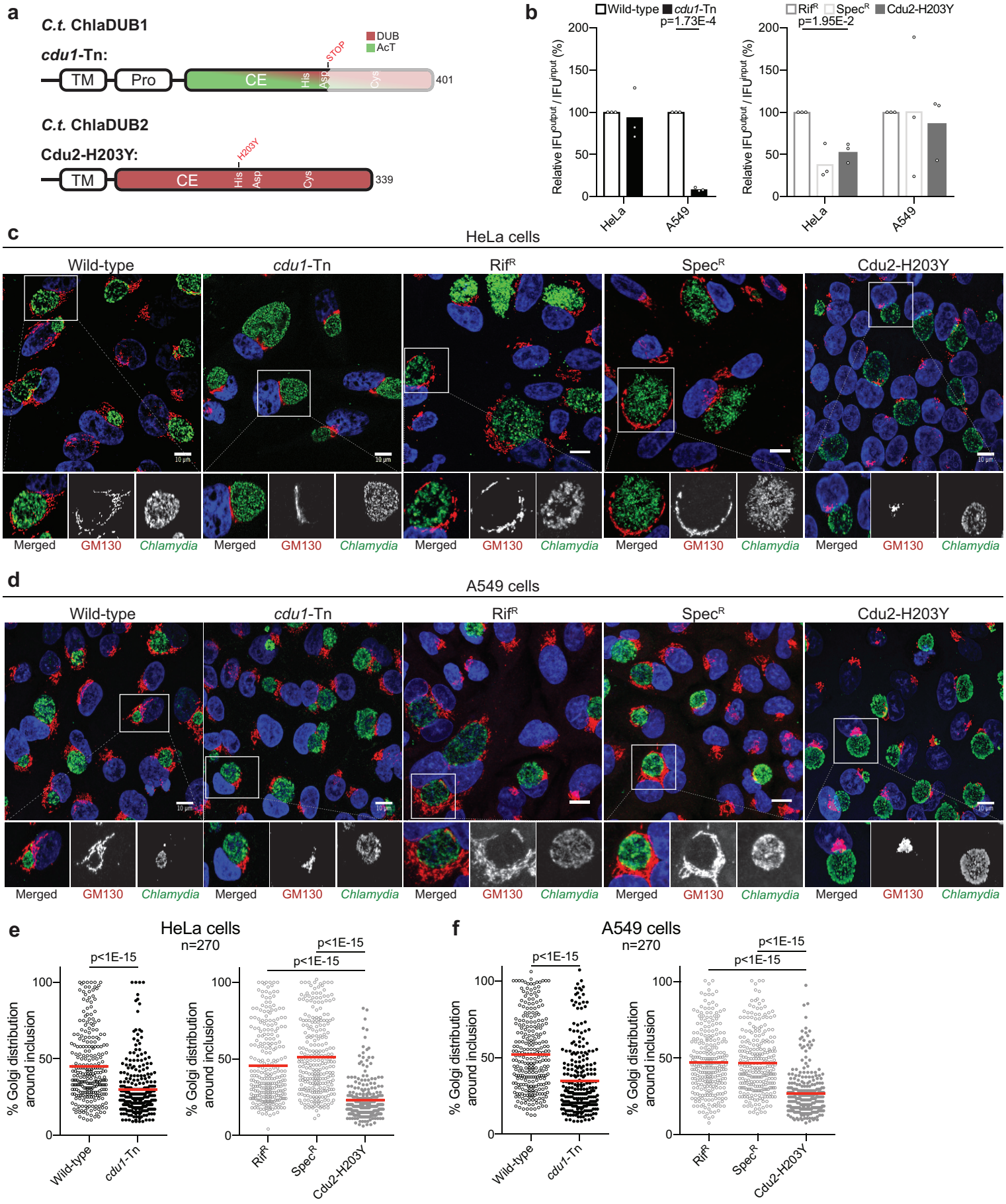

Figure 4: ChlaDUB deubiquitinase activity is responsible for Golgi fragmentation

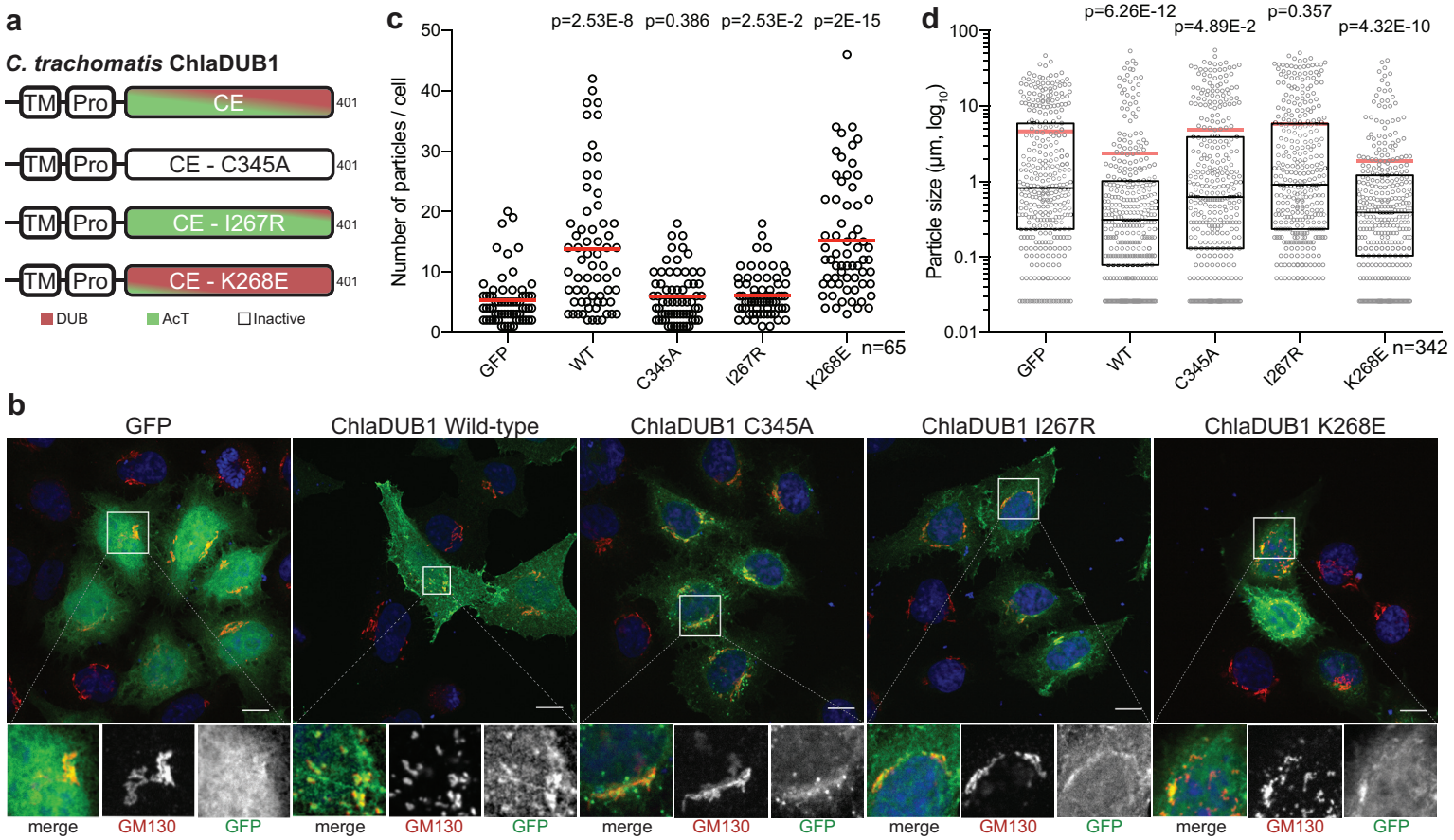

SUPPLEMENTARY INFORMATION

A *Chlamydia* effector combining deubiquitination and acetylation activities induces Golgi fragmentation

Jonathan N. Pruneda[1], Robert J. Bastidas[2‡], Erithelgi Bertsoulaki[3‡], Kirby N. Swatek[1], Balaji Santhanam[4], Michael J. Clague[3], Raphael H. Valdivia[2], Sylvie Urbé[3], and David Komander[1*]

[1] Division of Protein and Nucleic Acid Chemistry, MRC Laboratory of Molecular Biology, Francis Crick Avenue, Cambridge CB2 0QH, UK.

[2] Department of Molecular Genetics and Microbiology, Duke University, Durham, NC 27710, USA

[3] Cellular and Molecular Physiology, Institute of Translational Medicine, University of Liverpool, Crown Street, Liverpool L69 3BX, UK.

[4] Division of Structural Studies, MRC Laboratory of Molecular Biology, Francis Crick Avenue, Cambridge CB2 0QH, UK.

‡ These authors contributed equally

* Correspondence to: David Komander, dk@mrc-lmb.cam.ac.uk

Supplementary Figure 1: Identification of specialized and dual-function CE-clan enzymes

a) Extended time course following ChlaDUB1 acetyltransferase activity. Right, ^{14}C incorporation normalized to Coomassie stain, plotted over time. **b)** As in a), for GST-YopJ and substrate MEK2 in the absence and presence of activator IP6. **c)** As in a), for AvrA in the absence and presence of activator IP6. Full time course experiments shown in **a,b,c** were performed once but are representative of smaller scale experiments performed in triplicate. **d)** Anti-Acetyl-lysine Western blot analysis of ChlaDUB1 acetylation activity following overnight incubation with Acetyl-CoA. A representative gel is shown of duplicate experiments. **e)** 2 h incubation of ChlaDUB1 with ^{14}C Acetyl-CoA (0'), followed by 1 h incubation with H_2O, lysine deacetylase SIRT1, base (100 mM hydroxylamine in 100 mM bicine pH 9.0), or acid (1% formic acid). The histogram below plots the ^{14}C autoradiography signal normalized to the Coomassie stain as a difference compared to the 0' sample. Individual values and the average are shown. A representative gel is shown of triplicate experiments. **f)** Acetyltransferase assay testing the effect of YopJ/AvrA activator IP6 on ChlaDUB1 activity. The histogram below plots the ^{14}C autoradiography signal normalized to the Coomassie stain as a difference compared to the sample containing IP6. Individual values and the average are shown. A representative gel is shown of triplicate experiments. All uncropped gels are shown in Supplementary Fig. 10. **g)** Electrostatic surface potential (blue, positive charge; red, negative charge) showing the IP6 binding site on HopZ1a (pdb id 5KLQ) and the analogous region of ChlaDUB1 (pdb id 5HAG).

Supplementary Figure 1: Identification of specialized and dual-function CE-clan enzymes

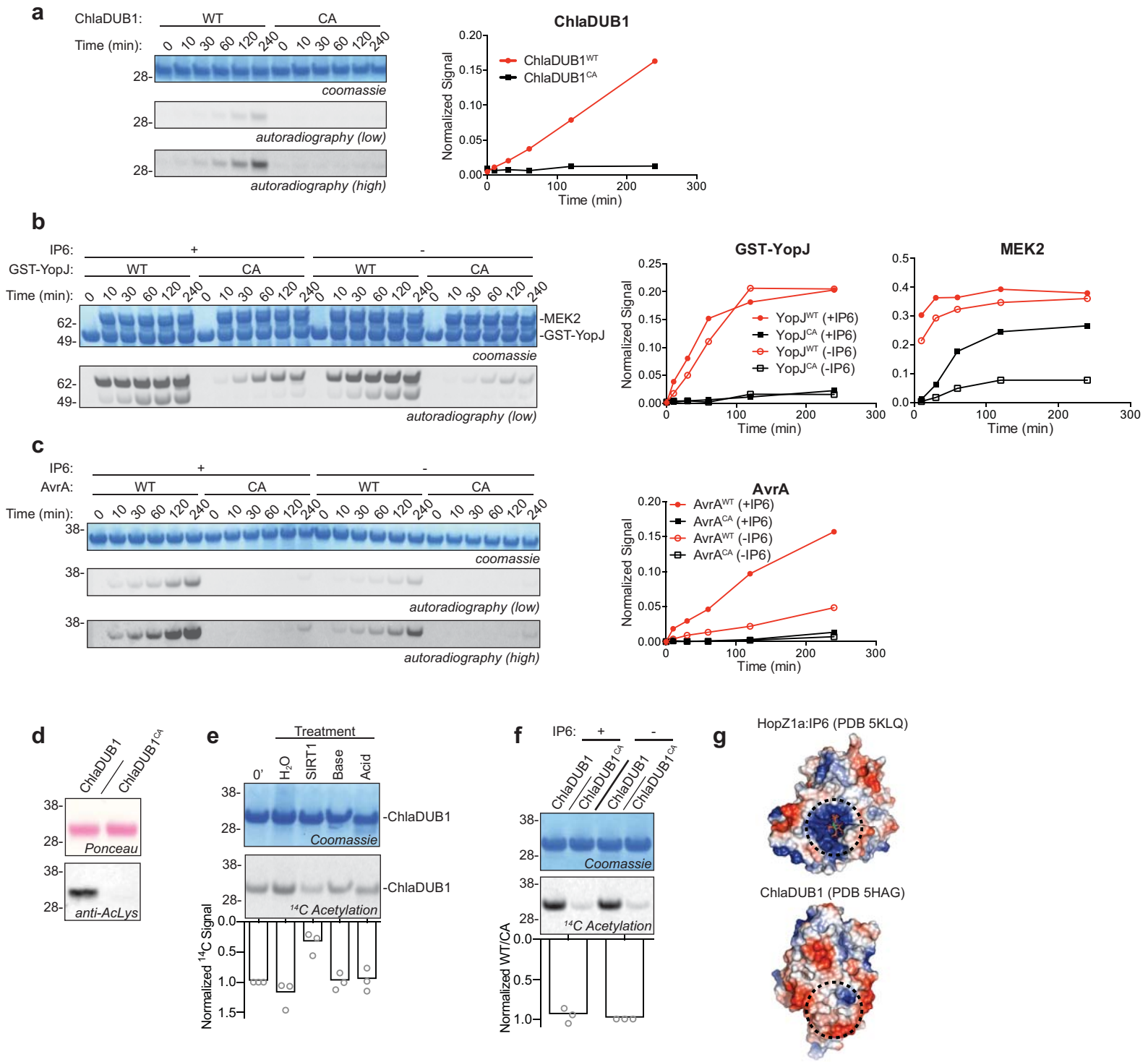

Supplementary Figure 2: Visualization and characterization of ChlaDUB1 dual activity

a) Superposition of the apo ChlaDUB1 (pdb id 5HAG), ChlaDUB1~Ub complex, and ChlaDUB1~CoA crystal structures showing only a slight movement (≤3Å Cα) in the VR-3 helix. 2|Fo|-|Fc| electron density contoured at 1σ is shown around the Ub C-terminus in the ChlaDUB1~Ub structure and around CoA of the ChlaDUB1~CoA structure. **b)** Full ASU of the 1.9Å ChlaDUB1~Ub structure showing 2|Fo|-|Fc| electron density contoured at 1σ **c)** Comparison of the ChlaDUB1~Ub complex to the eukaryotic SENP2-SUMO2 (pdb id 2IO0) and NEDP1~NEDD8 (pdb id 2BKR) complexes. The complex structures are aligned based upon the protease catalytic triad; only the conserved catalytic cores of SENP2 and NEDP1 are shown for clarity. **d)** Comparison of the ChlaDUB1~Ub complex to other bacterial DUB complexes, XopD~Ub (pdb id 5JP3) and SdeA~Ub (pdb id 5CRA). The complex structures are aligned based upon the protease catalytic triad; only the conserved catalytic cores of XopD and SdeA are shown for clarity. **e)** |Fo|-|Fc| omit map density (green, 2.5σ) for the CoA binding site in the 2.1Å ChlaDUB1~CoA crystal structure. **f)** Electrostatic surface potential (blue, positive charge; red, negative charge) illustrating charge complementarity within the CoA binding site. **g)** Comparison of the ChlaDUB1~CoA complex with the YopJ-like acetyltransferase HopZ1a~CoA (pdb id 5KLQ), and the human (pdb id 2PFR) and *Mycobacterium marinum* (pdb id 2VFC) arylamine N-acetyltransferases (NATs), aligned *via* their catalytic triads. **h)** CoA molecules from the structures shown in g) superposed onto the ChlaDUB1~CoA crystal structure. **i)** Secondary structure diagram illustrating the variable regions unique to ChlaDUB1, and their contributions to the Ub (red) and CoA (green) binding sites.

Supplementary Figure 2: Visualization and characterization of ChlaDUB1 dual activity

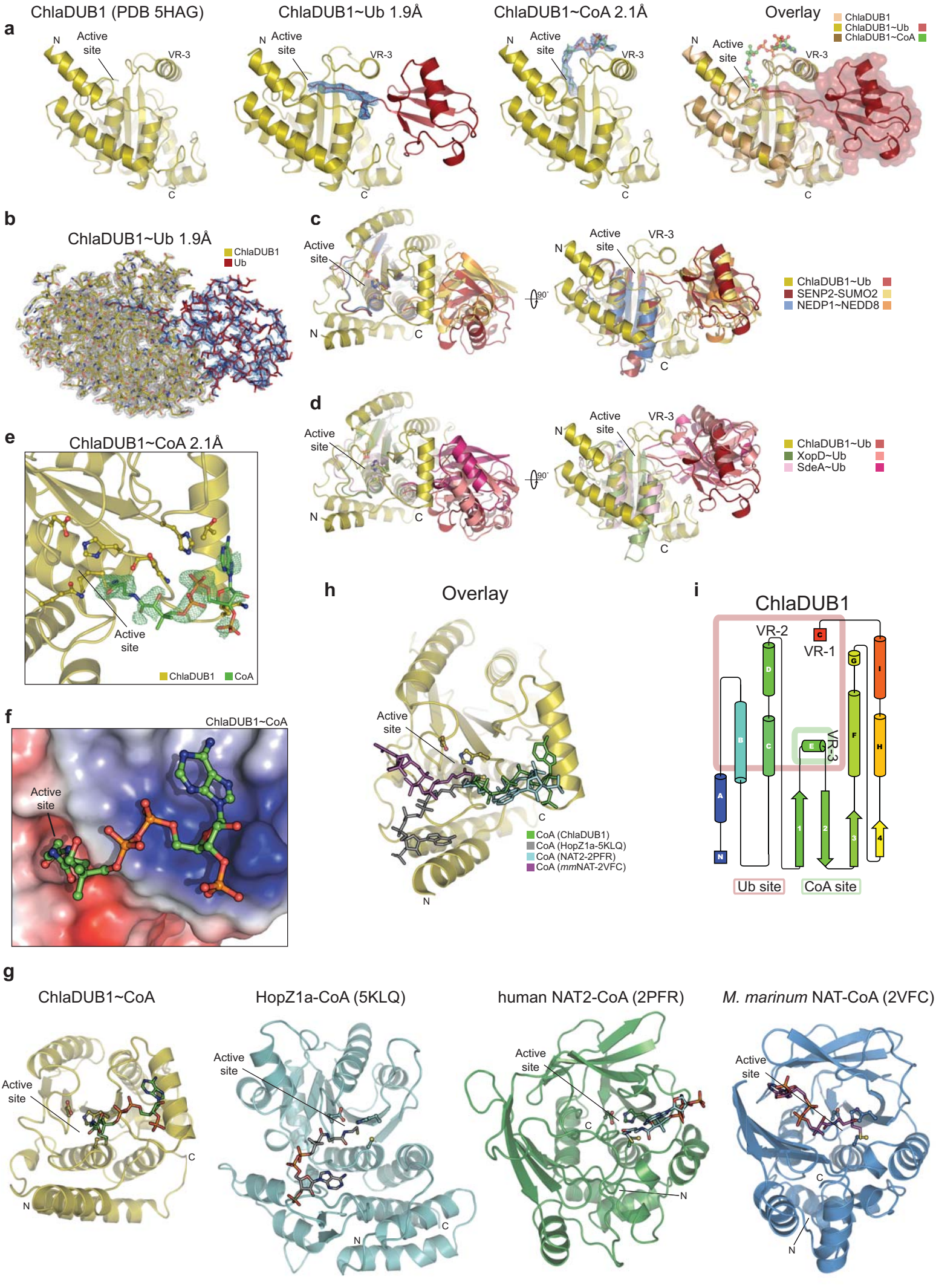

Supplementary Figure 3: Reaction schematic for ChlaDUB1 DUB and AcT activities

Proposed reaction scheme illustrating how ChlaDUB1 could mediate key steps for deubiquitination (left) and acetylation (right), including i) nucleophilic attack, ii) the acyl-enzyme intermediate, and iii) resolution back to the apo enzyme following attack by water (DUB) or substrate Lys (AcT). States outlined in black correspond to the intermediates captured in the ChlaDUB1~Ub and ChlaDUB1~CoA crystal structures.

Supplementary Figure 3: Reaction schematic of ChlaDUB1 DUB and AcT activities

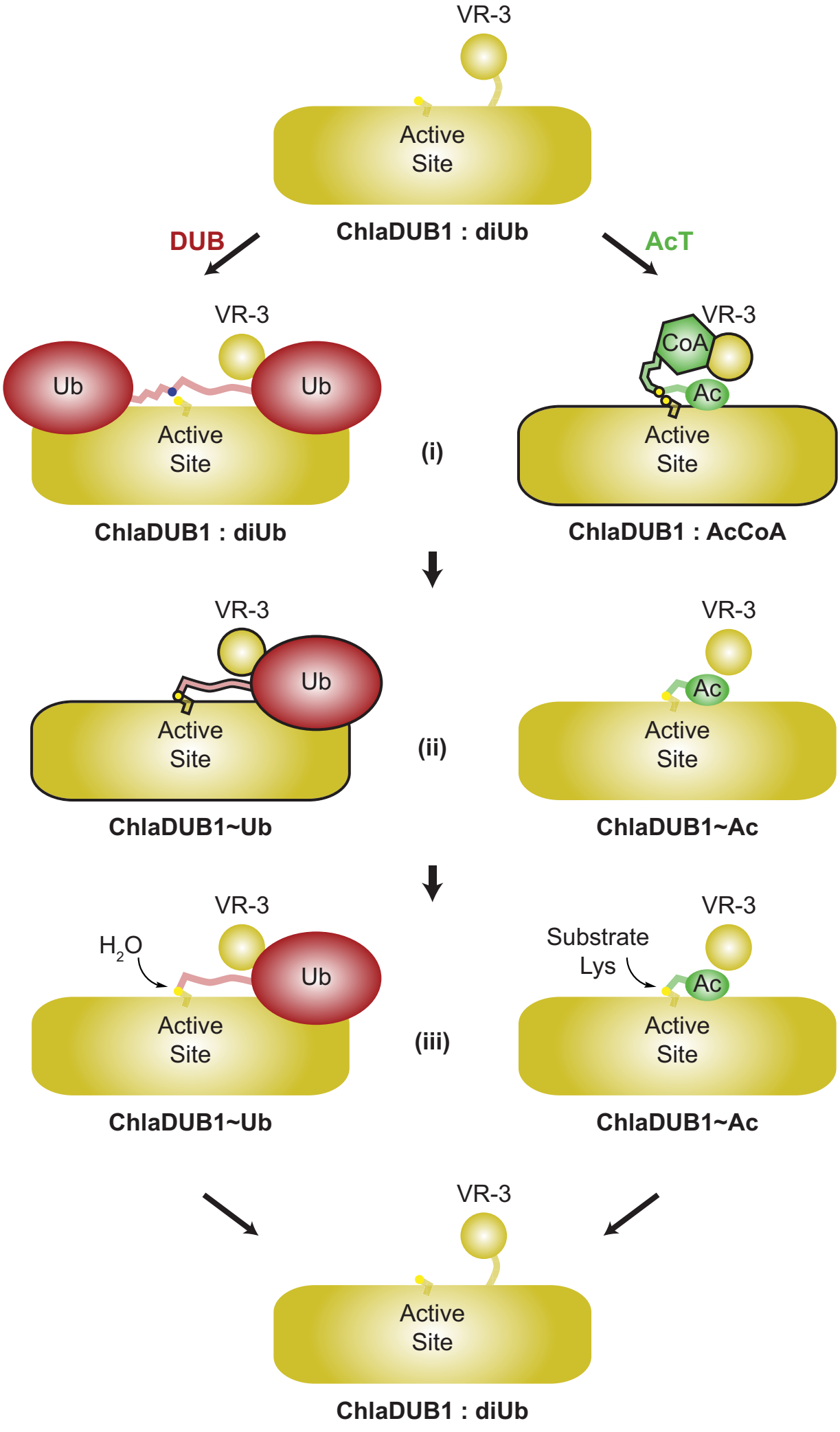

Supplementary Figure 4: DUB and AcT requirements in the ChlaDUB1 active site

a) K63-linked diUb deubiquitinase assay showing a dependence upon the ChlaDUB1 catalytic Cys (C345), general base His (H275), and oxyanion hole Gln (Q338). A representative gel is shown of triplicate experiments. **b)** As in a), for a ^{14}C acetylation assay. A representative gel is shown of triplicate experiments. **c)** ChlaDUB1 acetylation assay in the presence of increasing concentrations of wild-type Ub (aa 1-76) or UbΔC (aa 1-72). A representative gel is shown of duplicate experiments. All uncropped gels are shown in Supplementary Fig. 10.

Supplementary Figure 4: DUB and AcT requiremens in the ChlaDUB1 active site

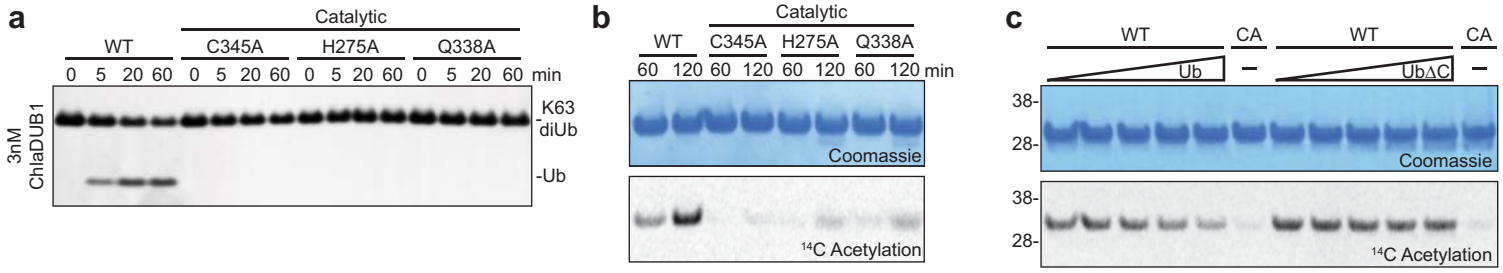

Supplementary Figure 5: Molecular dissection of dual deubiquitinase/acetyltransferase activities

a) Cleavage of the KG-TAMRA-linked Ub substrate by wild-type and mutant ChlaDUB1 monitored by change in fluorescence polarization over time. **b)** Deubiquitinase assay comparing *C.t.* ChlaDUB1 activity against *C.t.* ChlaDUB2 and *C.a.* ChlaDUB. Enzyme concentrations were adjusted to produce qualitatively similar rates of cleavage. Uncropped gels are shown in Supplementary Fig. 10. **c)** Comparison of activity and specificity for *C.t.* ChlaDUB1, *C.t.* ChlaDUB2, and *C.a.* ChlaDUB using the KG-TAMRA-linked Ub/Ubl substrates. All enzymes were held at a high concentration to illustrate differences in cleavage rates. Data in **a,b,c** are representative of assays performed in triplicate. **d)** 1.5 Å crystal structure of *C.a.* ChlaDUB with active site residues shown in ball-and-stick. The structure revealed an unexpected His-Cys-His-Cys Zn^{2+} binding site located in VR-2. Any significance of this metal binding beyond a structural role is unknown. Inlay, close-up view showing Zn^{2+}-coordinating residues, along with 2|Fo|-|Fc| electron density contoured at 1σ. Right, secondary structure diagram illustrating the variable regions unique to *C.a.* ChlaDUB, and their contributions to the CoA S1' site (green). Structure boundaries are annotated. **e)** Sequence alignment of *Chlamydia* ChlaDUB orthologues focusing on the region surrounding the *C.a.* ChlaDUB Zn^{2+}-binding site. ChlaDUB orthologues roughly segregate into three groups: 1) ChlaDUB1 members that lack any apparent Zn^{2+}-coordinating residues, 2) ChlaDUB2 members that encode a conserved set of four, potentially Zn^{2+}-coordinating Cys residues (grey arrows), and 3) ChlaDUB members that encode a conserved HCHC Zn^{2+}-binding motif as observed in *C.a.* ChlaDUB (red arrows). Numbering corresponds to the *C.t.* ChlaDUB1 sequence.

Supplementary Figure 5: Molecular dissection of dual deubiquitinase/acetyltransferase activities

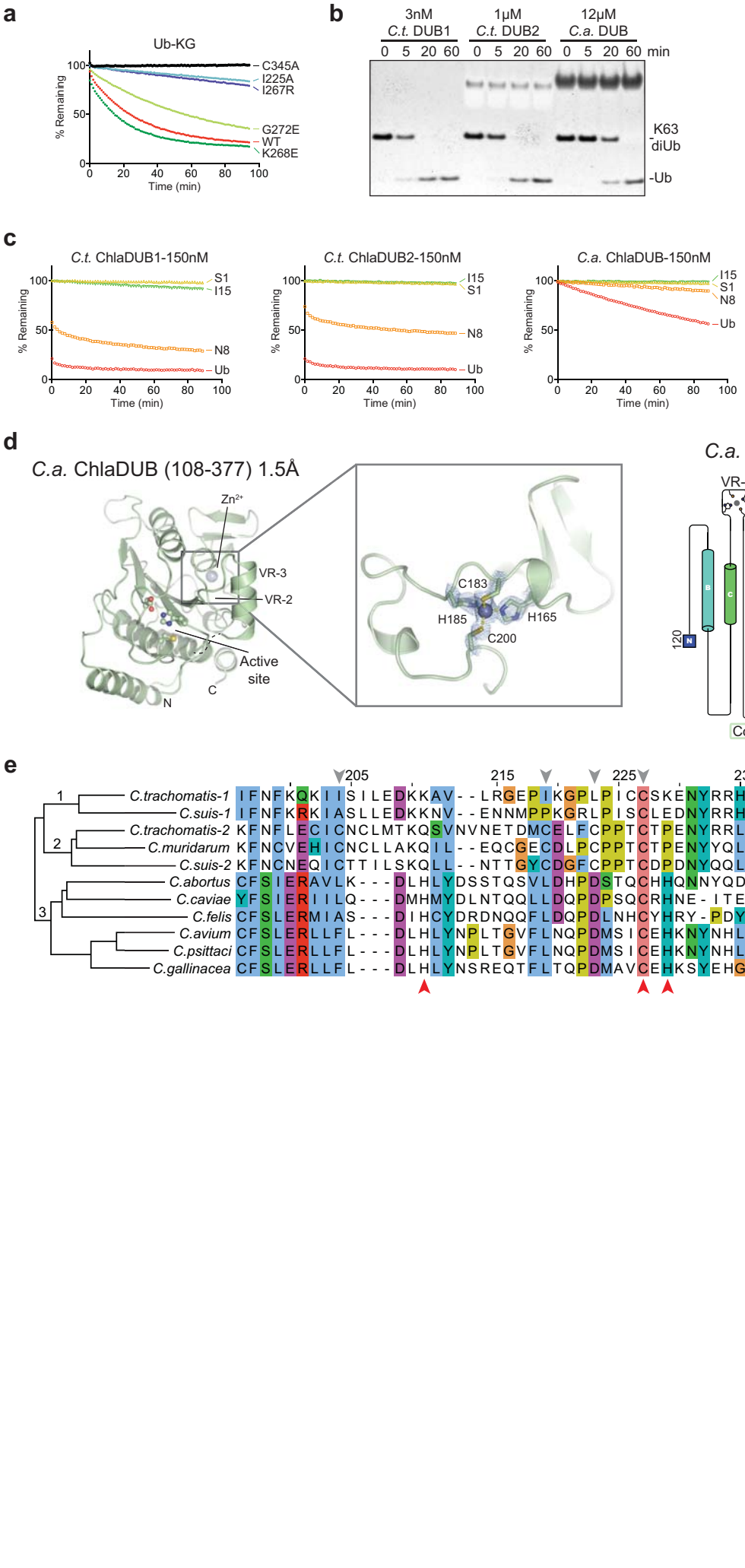

Supplementary Figure 6: ChlaDUB deubiquitinase activity is required for *C. trachomatis* Golgi fragmentation

a) Deubiquitinase assay comparing the activities of wild-type and H203Y ChlaDUB2 against K63-linked diUb. A representative gel is shown of triplicate experiments. Uncropped gels are shown in Supplementary Fig. 10. **b)** Representative confocal images showing Golgi fragmentation and redistribution around the *Chlamydia* inclusion following infection of HeLa cells. Samples were immunostained with anti-GM130 (cis-Golgi, red) and anti-Slc1 (*Chlamydia*, green) antibodies, and Hoechst stained (DNA, blue). Scale bar corresponds to 10 μm. **c)** As in b) for A549 cells. **d)** Quantification of Golgi fragmentation, as shown in Fig. 3e, for individual biological replicates. Mean values are shown as a red bar with individual data points overlaid. **e)** As in d) for A549 cells.

Supplementary Figure 6: ChlaDUB function is required for *C. trachomatis* Golgi fragmentation

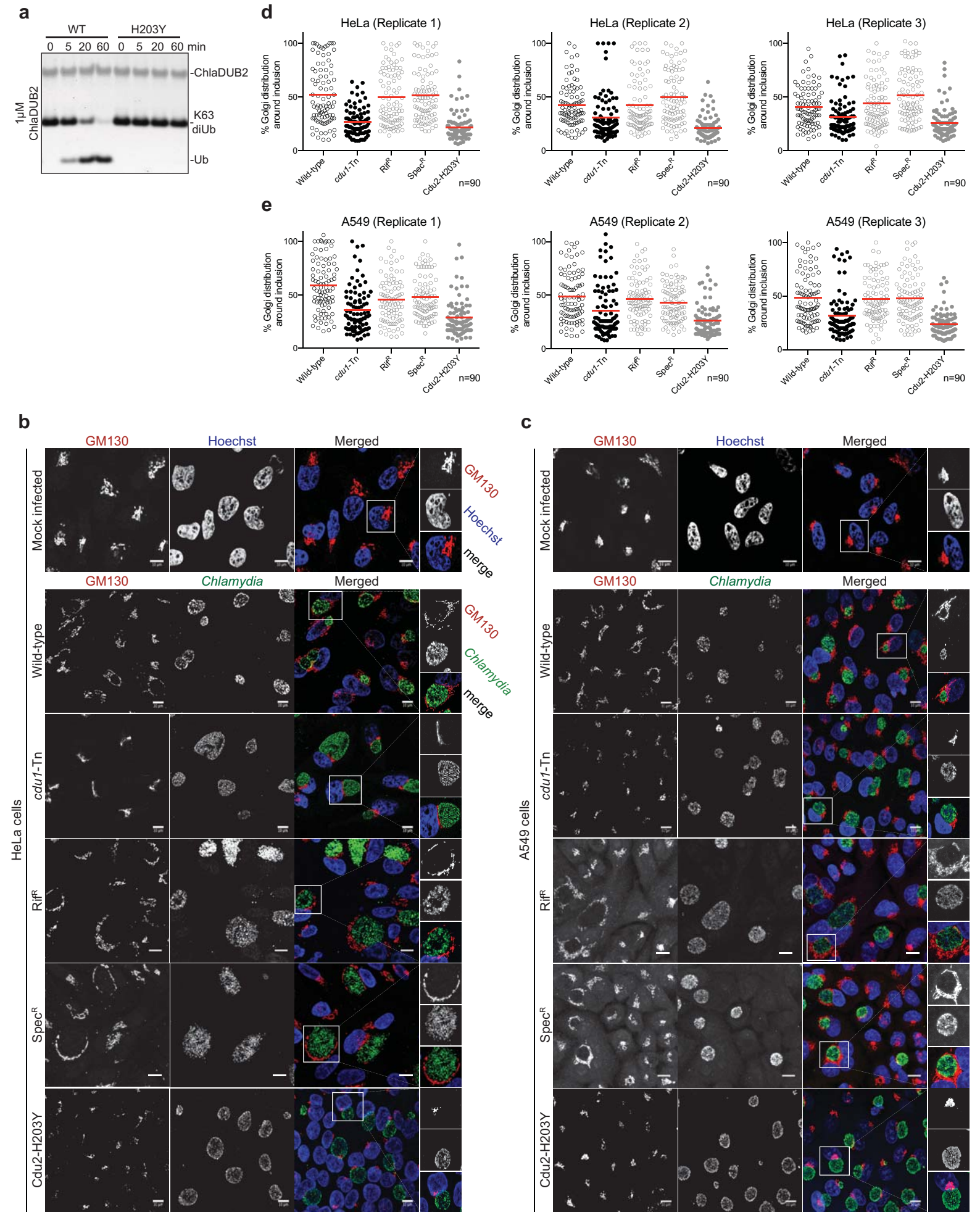

Supplementary Figure 7: ChlaDUB1 deubiquitinase activity is required for *C. trachomatis* Golgi fragmentation

a) Anti-GFP Western blot illustrating equal expression of GFP-ChlaDUB1 wild-type and point mutants. The inactive ChlaDUB1 C345A appears to be mono-ubiquitinated. A representative blot is shown of duplicate experiments. Uncropped gels are shown in Supplementary Fig. 10. **b)** Representative confocal images showing Golgi fragmentation in HeLa cells following expression of GFP-tagged ChlaDUB1. Samples were immunostained with anti-GM130 (cis-Golgi, red) and DAPI stained (DNA, blue). GFP fluorescence is shown in green. Scale bar corresponds to 10 μm. **c)** Quantification of Golgi puncta, as in Fig. 4c, for additional two biological replicates. Mean values are shown as red bars with individual data points overlaid. Statistical significance compared to GFP control was measured using a two-tailed Mann-Whitney test. Replicate 2: GFP – WT, p=9.40E-9; GFP – C345A, p=0.256; GFP – I267R, p=0.958; GFP – K268E, p=4.29E-6. Replicate 3: GFP – WT, p=1.0E-14; GFP – C345A, p=0.579; GFP – I267R, p=0.0276; GFP – K268E, p=5.07E-7. **d)** Quantification of Golgi puncta size, as in Fig. 4d, for additional two biological replicates. Mean values are shown as red bars, median values are shown as black bars inside a quartile box plot, with individual data points overlaid. Statistical significance compared to GFP control was measured using a two-tailed Mann-Whitney test. Replicate 2: GFP – WT, p<1E-15; GFP – C345A, p=0.655; GFP – I267R, p=0.863; GFP – K268E, p=0.000131. Replicate 3: GFP – WT, p<1E-15; GFP – C345A, p=0.181; GFP – I267R, p=0.306; GFP – K268E, p<1E-15.

Supplementary Figure 7: ChlaDUB1 deubiquitinase activity is responsible for Golgi fragmentation

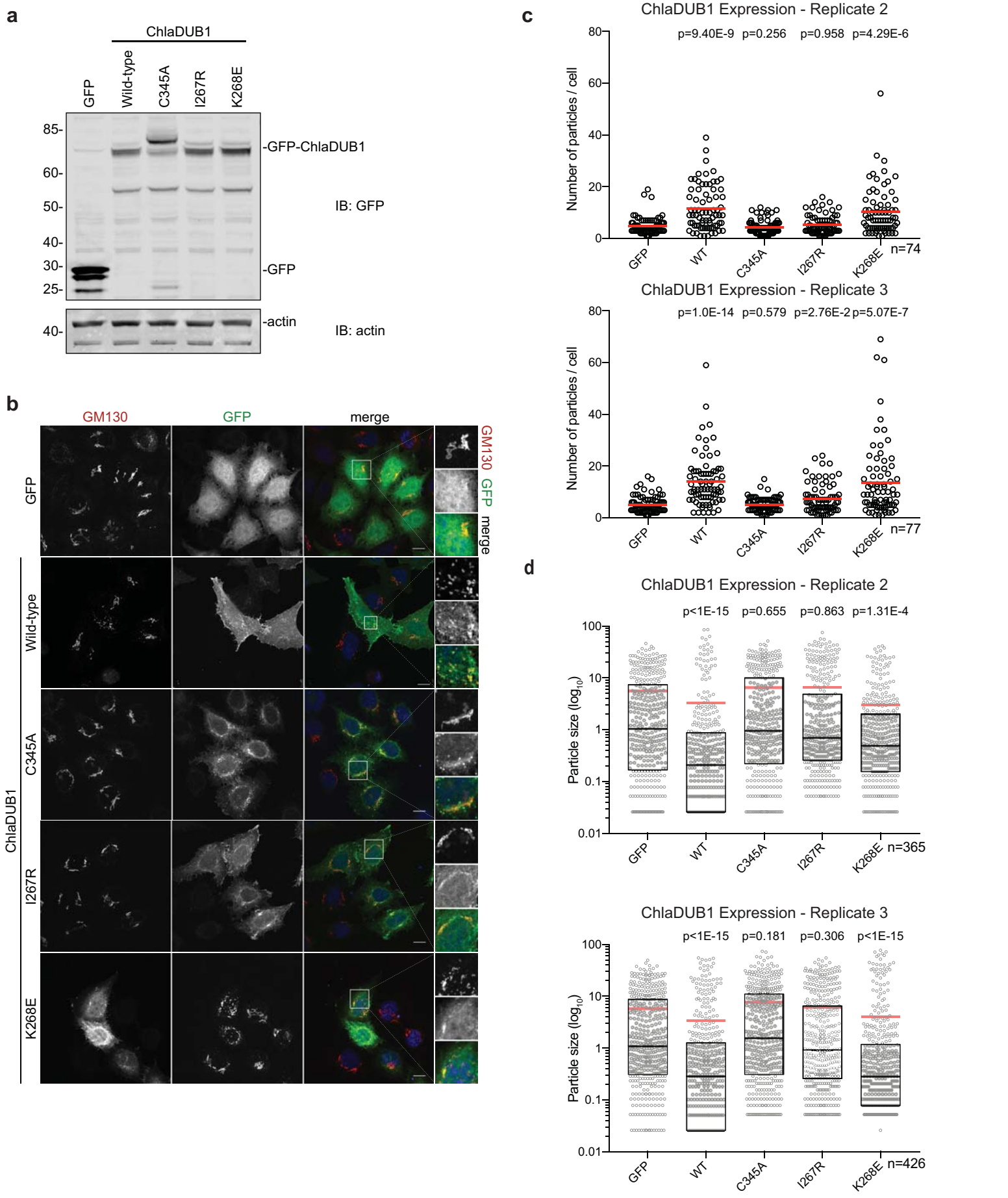

Supplementary Figure 8: ChlaDUB2 deubiquitinase activity is required for *C. trachomatis* Golgi fragmentation.

a) Anti-GFP Western blot illustrating equal expression of GFP-ChlaDUB2 wild-type and point mutants. The inactive ChlaDUB2 C282A appears to be mono-ubiquitinated. A representative blot is shown of duplicate experiments. Uncropped gels are shown in Supplementary Fig. 10. **b)** Representative confocal images of experiments performed in triplicate showing Golgi fragmentation in HeLa cells following expression of GFP-tagged ChlaDUB2. Samples were immunostained with anti-GM130 (cis-Golgi, red) and DAPI stained (DNA, blue). GFP fluorescence is shown in green. Scale bar corresponds to 10 μm. **c)** Quantification of Golgi puncta, as in Fig. 4c, for all three biological replicates of ChlaDUB2 expression. Mean values are shown as red bars with individual data points overlaid. Statistical significance compared to GFP control was measured using a two-tailed Mann-Whitney test. GFP – WT, p=0.00239; GFP – C282A, p=0.0660; GFP – H203Y, p=0.102. **d)** Quantification of Golgi puncta size, as in Fig. 4d, for all three biological replicates of ChlaDUB2 expression. Mean values are shown as red bars, median values are shown as black bars inside a quartile box plot, with individual data points overlaid. Statistical significance compared to GFP control was measured using a two-tailed Mann-Whitney test. GFP – WT, p=1.95E-6; GFP – C282A, p=2.98E-12; GFP – H203Y, p=3.16E-7. **e)** Representative images of experiments performed in triplicate demonstrating co-localization of ChlaDUB2 constructs with a mCherry-KDL reporter of the ER.

Supplementary Figure 8: ChlaDUB2 deubiquitinase activity is responsible for Golgi fragmentation

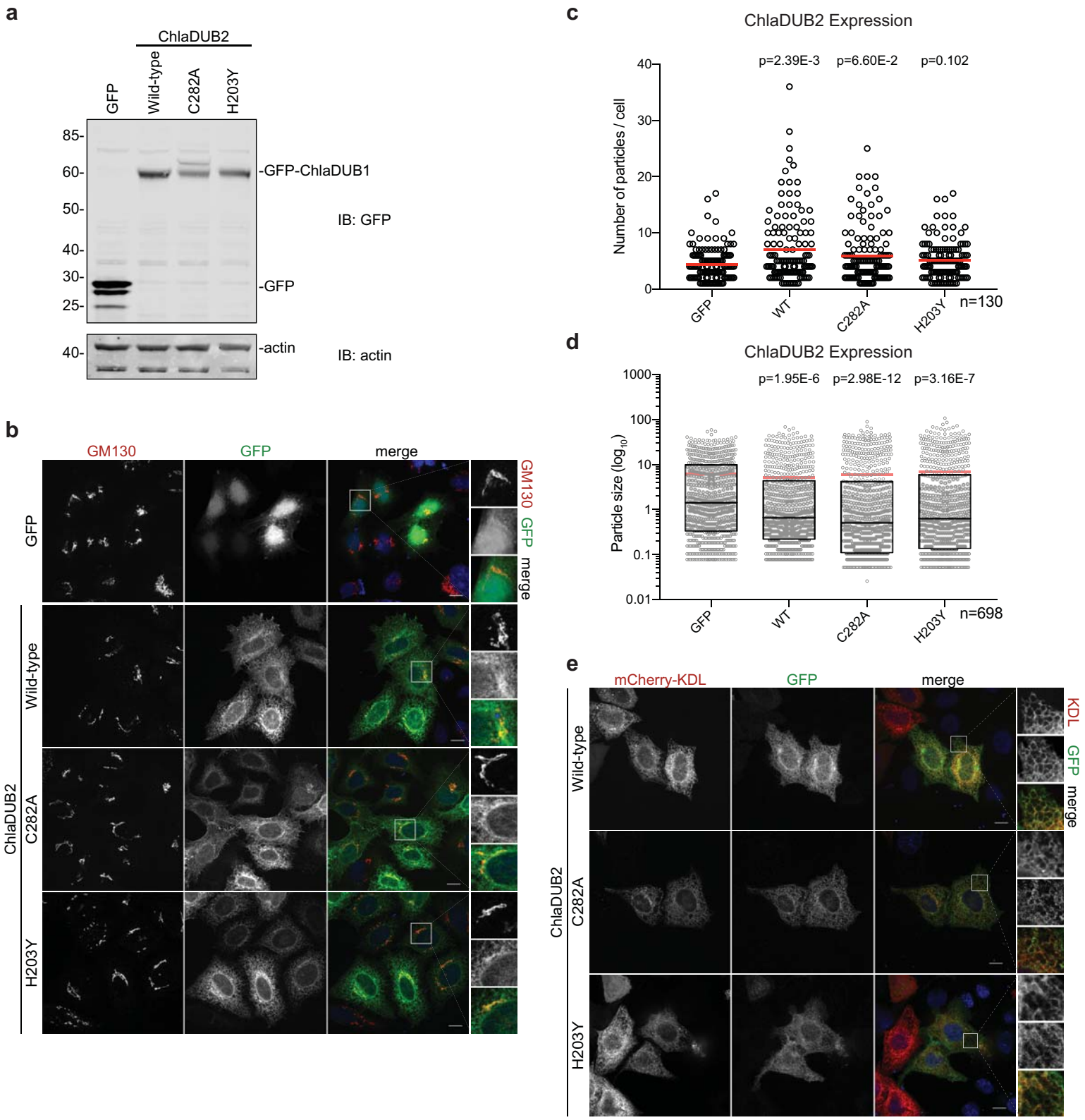

Supplementary Figure 9: ChlaDUB1 DUB activity in the context of *Chlamydia* infection

Illustration of ChlaDUB1 dual activity in the context of *Chlamydia* infection. At approximately 20 hours post infection, the *Chlamydia* inclusion has re-localized to the microtubule-organizing center, where active bacterial replication begins. At this time, ChlaDUB1 and ChlaDUB2 are expressed and secreted into the host cell, where they insert into the inclusion membrane[15,27]. The DUB activities of both ChlaDUB effector proteins is required for fragmentation of the host Golgi apparatus (shown herein), which redistributes around the inclusion to facilitate *Chlamydia* replication[24]. InaC, another *Chlamydia* effector localized to the outside of the inclusion, recruits host 14-3-3 proteins and ADP ribosylation factors (ARFs)[23] to promote Golgi redistribution around the inclusion by stabilizing the surrounding microtubule network through alpha-tubulin detyrosination and acetylation[26]. Host GTPases Rab6A and Rab11A are also recruited to the *Chlamydia* inclusion to regulate Golgi fragmentation[27], but how they are recruited and the role they play upon arrival remain to be determined. Targets of the ChlaDUB1 AcT activity and their contributions to *Chlamydia* biology also remain unknown, though ChlaDUB1 has been implicated in other host processes such as suppression of NF-κB signaling[13] and cell death[15], and the activity responsible for these interactions remains to be established.

Supplementary Figure 9: ChlaDUB1 DUB activity in the context of *Chlamydia* infection

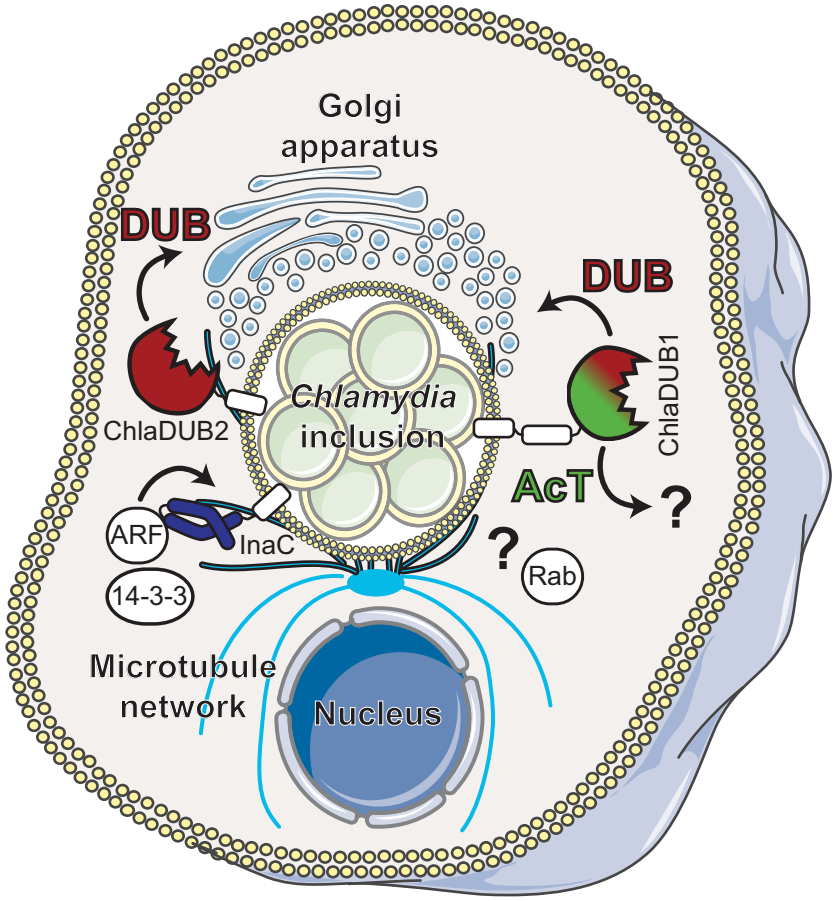

Supplementary Figure 10: Uncropped gels

Main Figures

1a

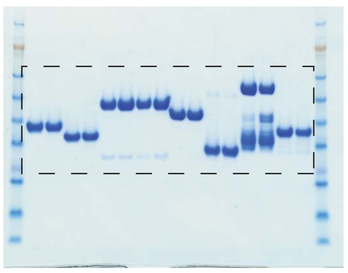

1b

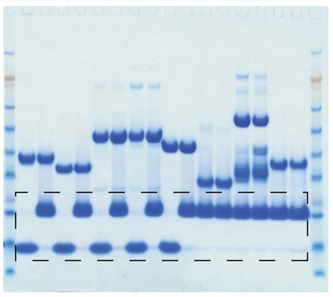

1c

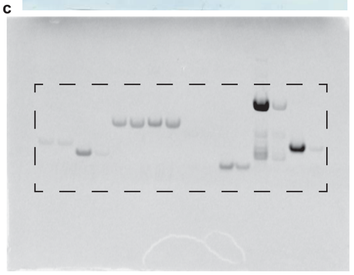

2c

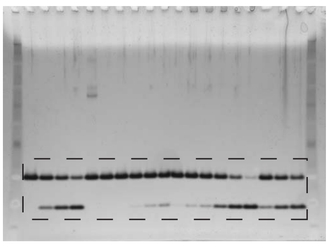

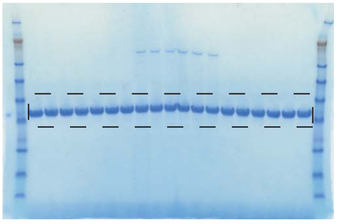

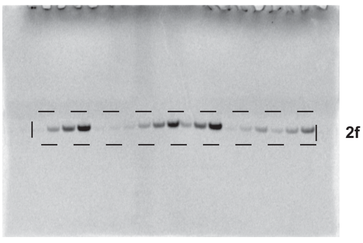

2e

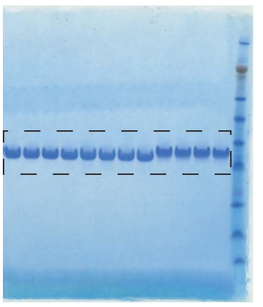

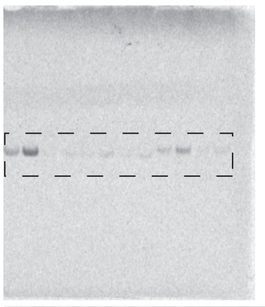

2f

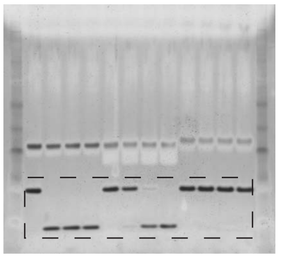

Supplementary Figures

1a

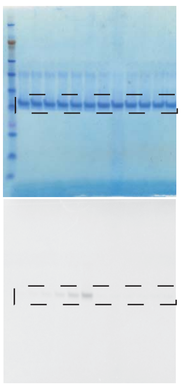

1b

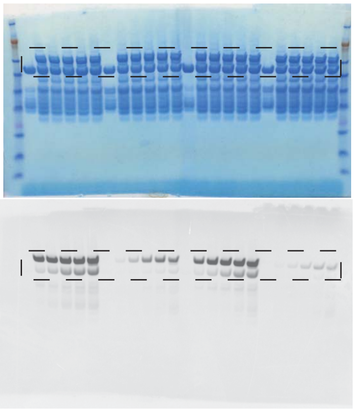

1c

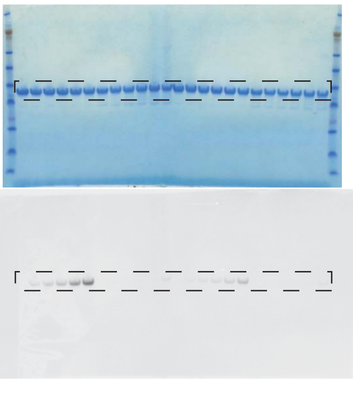

1d

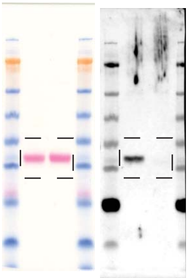

1e

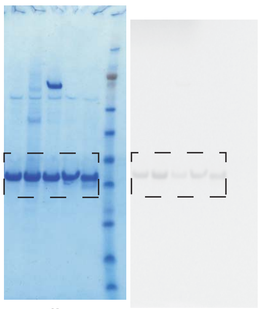

1f

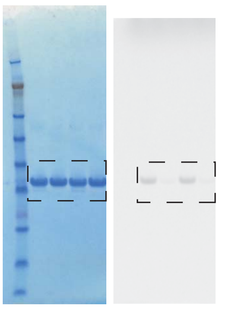

4a

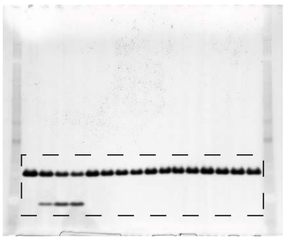

4b

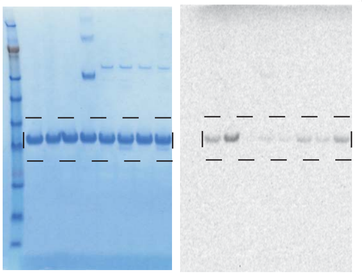

4c

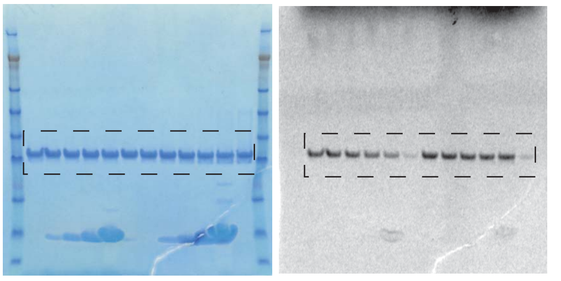

5b

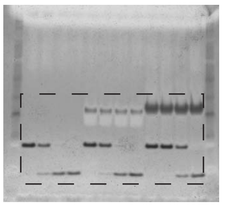

6a

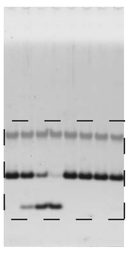

7a

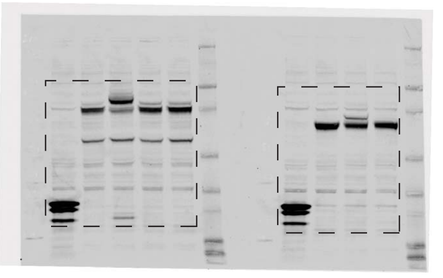

8a

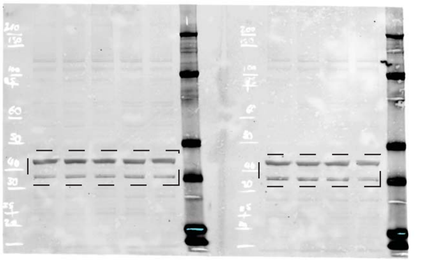

Supplementary Table 1: Data collection and refinement statistics

	ChlaDUB1~Ub SeMet	ChlaDUB1~Ub	ChlaDUB1~CoA	*C.a.* ChlaDUB
Data collection				
Space group	*P* 2_1	*P* 2_1	*I* 2 3	*P* 1
Cell dimensions				
a, *b*, *c* (Å)	54.09, 55.57, 60.17	53.8, 55.77, 58.57	132.63, 132.63, 132.63	40.34, 41.78, 44.21
α, β, γ (°)	90, 95.6, 90	90, 93.57, 90	90, 90, 90	94.72, 102.17, 101.23
Wavelength (Å)	0.9798 (peak)			
Resolution (Å)	27.78-2.00 (2.05-2.00)	26.85-1.90 (1.94-1.90)	66.32-2.10 (2.16-2.10)	42.86-1.47 (1.50-1.47)
R_{merge}	0.064 (1.0)	0.043 (0.476)	0.085 (0.653)	0.063 (0.471)
$I / \sigma I$	24.3 (3.0)	12.4 (2.4)	10.3 (2.1)	8.4 (2.0)
Completeness (%)	100.0 (100.0)	99.9 (100.0)	99.9 (100.0)	96.4 (94.2)
Redundancy	17.1 (17.5)	3.4 (3.4)	5.1 (5.2)	3.6 (3.7)
Refinement				
Resolution (Å)		26.85-1.90	66.32-2.10	42.86-1.47
No. reflections		93418	116341	162381
R_{work} / R_{free}		18.1 / 21.3	18.2 / 21.6	15.2 / 18.2
No. atoms				
Protein		2515	2140	1937
Ligand/ion		15	77	7
Water		184	147	192
B-factors				
Protein		60.7	29.2	30.4
Ligand/ion		66.4	54.2	39.7
Water		48.7	36.2	41.1
R.m.s. deviations				
Bond lengths (Å)		0.010	0.011	0.014
Bond angles (°)		1.38	1.12	1.56

One crystal was used per data collection. *Values in parentheses are for highest-resolution shell.

Supplementary Table 2: Strains used in this study

Strain name	Mutant locus	Mutant gene	Protein name	Base pair substitution*	Amino acid substitution	Source
LGV L2 434/Bu (Wild-type)						Reference strain
cdu1-Tn	CTL0247	*cdu1*	ChlaDUB1/Cdu1		Y297*	Fischer et al., 2017[15]
Rif^R LGV L2 434 Bu						Nguyen et al.,2012[40]
$Spec^R$ LGV L2 434 Bu						Nguyen et al.,2012[40]
CTL2M467 rs22 (Cdu2-H203Y)	CTL0246	*cdu2*	ChlaDUB2/Cdu2	*G607A*	H203Y	This study

* Base pair substitution induced by EMS mutagenesis (Kokes et al., 2015)[23].

Supplementary Table 3: M467 rs22 single nucleotide variants

a) Single nucleotide variants (SNVs) present in M467 rs22 parental strain CTL2M467 generated in Kokes et al[23].

Genome position	Locus tag	Gene name	SNV type	Base pair substitution	Amino acid substitution
303169	CTL0246	*cdu2*	Non synonymous	*G607A*	H203Y
79831	CTL0066	*nth*	Non synonymous	*G463A*	L155F
214963	CTL0166	*pgsA*	Synonymous	*G345A*	
33473	CTL0027	*sfhB*	Non synonymous	*C191T*	S64F
55081			Non coding	*G55081A*	
142623			Non coding	*G142623A*	

Variants identified by whole genome sequencing.

b) CTL2M467 non synonymous SNVs inherited by recombinant strain M467 rs22.

Genome position	Locus tag	Gene name	SNV type	Base pair substitution	Amino acid substitution
303169	CTL0246	*cdu2*	Non synonymous	*G607A*	H203Y

Variants identified by PCR based genotyping.